International Journal of Nanomedicine

Dovepress
open access to scientific and medical research

Open Access Full Text Article

ORIGINAL RESEARCH

ULK1 Mediated Autophagy-Promoting Effects of Rutin-Loaded Chitosan Nanoparticles Contribute to the Activation of NF-κB Signaling Besides Inhibiting EMT in Hep3B Hepatoma Cells

Peng Wu[1]*, Xiaoyong Wang[2]*, Min Yin[1]*, Wenjie Zhu[3]*, Zheng Chen[1], Yang Zhang[1], Ziyu Jiang[4], Longqing Shi[5], Qiang Zhu[1]

[1]Children's Hospital of Nanjing Medical University, Nanjing, People's Republic of China; [2]The People's Hospital of Rugao, Nantong, People's Republic of China; [3]Kangda College of Nanjing Medical University, Nanjing, People's Republic of China; [4]Department of Oncology, Affiliated Hospital of Integrated Traditional Chinese and Western Medicine, Nanjing University of Chinese Medicine, Nanjing, 210028, People's Republic of China; [5]Department of Hepatobiliary and Pancreatic Surgery, Third Affiliated Hospital of Soochow University, Jiangsu, People's Republic of China

*These authors contributed equally to this work

Correspondence: Longqing Shi, Department of Hepatobiliary and Pancreatic Surgery, The Third Affiliated Hospital of Soochow University, Jiangsu, People's Republic of China, Email 20204135017@stu.suda.edu.cn; Qiang Zhu, Children's Hospital of Nanjing Medical University, Nanjing, People's Republic of China, Email zhu20081023@yeah.net

Background: Liver cancer remains to be one of the leading causes of cancer worldwide. The treatment options face several challenges and nanomaterials have proven to improve the bioavailability of several drug candidates and their applications in nanomedicine. Specifically, chitosan nanoparticles (CNPs) are extremely biodegradable, pose enhanced biocompatibility and are considered safe for use in medicine.

Methods: CNPs were synthesized by ionic gelation, loaded with rutin (rCNPs) and characterized by ultraviolet–visible spectroscopy (UV-Vis), Fourier-transform infrared spectroscopy (FTIR), dynamic light scattering (DLS) and transmission electron microscopy (TEM). The rCNPs were tested for their cytotoxic effects on human hepatoma Hep3B cells, and experiments were conducted to determine the mechanism of such effects. Further, the biocompatibility of the rCNPs was tested on L929 fibroblasts, and their hemocompatibility was determined.

Results: Initially, UV–vis and FTIR analyses indicated the possible loading of rutin on rCNPs. Further, the rutin load was quantitatively measured using Ultra-Performance Liquid Chromatography (UPLC) and the concentration was 88 µg/mL for 0.22 micron filtered rCNPs. The drug loading capacity (LC%) of the rCNPs was observed to be 13.29 ± 0.68%, and encapsulation efficiency (EE%) was 19.55 ± 1.01%. The drug release was pH-responsive as 88.58% of the drug was released after 24 hrs at the lysosomal pH 5.5, whereas 91.44% of the drug was released at physiological pH 7.4 after 102 hrs. The cytotoxic effects were prominent in 0.22 micron filtered samples of 5 mg/mL rutin precursor. The particle size for the rCNPs at this concentration was 144.1 nm and the polydispersity index (PDI) was 0.244, which is deemed to be ideal for tumor targeting. A zeta potential (ζ-potential) value of 16.4 mV indicated rCNPs with good stability. The IC_{50} value for the cytotoxic effects of rCNPs on human hepatoma Hep3B cells was 9.7 ± 0.19 µg/mL of rutin load. In addition, the increased production of reactive oxygen species (ROS) and changes in mitochondrial membrane potential (MMP) were observed. Gene expression studies indicated that the mechanism for cytotoxic effects of rCNPs on Hep3B cells was due to the activation of Unc-51-like autophagy-activating kinase (ULK1) mediated autophagy and nuclear factor kappa B (NF-κB) signaling besides inhibiting the epithelial–mesenchymal Transition (EMT). In addition, the rCNPs were less toxic on NCTC clone 929 (L929) fibroblasts in comparison to the Hep3B cells and possessed excellent hemocompatibility (less than 2% of hemolysis).

Conclusion: The synthesized rCNPs were pH-responsive and possessed the physicochemical properties suitable for tumor targeting. The particles were effectively cytotoxic on Hep3B cells in comparison to normal cells and possessed excellent hemocompatibility. The very low hemolytic profile of rCNPs indicates that the drug could be administered intravenously for cancer therapy.

Received: 4 October 2023
Accepted: 8 May 2024
Published: 18 May 2024

Keywords: rCNPs, Hep3B, ROS, qPCR, mechanism

Introduction

Cancer is an ever-growing global burden with more than 10 million new cases and 7 million deaths that occurred in 2007. The global predictions are expected to rise to around 26 million new cases and 17 million deaths for the year 2030. This burden will increase in low- and middle-income countries up to 61% of the global cases in 2050.[1] In this regard, liver cancer is one of the leading causes for global deaths with more than 0.8 million deaths globally.[2] It ranks second after lung cancer in being a cause for premature deaths in the year 2020 as more than 0.5 million deaths occurred between the ages 30 and 69 with poor survival rate. The cases may rise to more than 55% by the year 2040 (1.4 million new cases from 0.8 million cases in 2020). The deaths related to liver cancer are projected to rise to 1.3 million by 2040.[3]

Adding to this, the estimated new cases related to liver cancer are 41,210, and the death toll is projected at 29,380 for the year 2023 across the United States.[4] In China, the projected new cases for the year 2022 related to liver cancer were 431,383, while the deaths were projected at 412,216.[5] The current treatment options for liver cancer include surgical removal and/or replacement of the organ for having a liver transplant, fulguration, transarterial chemoembolization (blockage of blood supply to the tumor tissue), radioembolization and systemic targeting using kinase inhibitor drugs in combination with monoclonal antibodies.[6,7] Poor solubility in aqueous solutions, non-specific targeting of normal and healthy tissues resulting in harmful side-effects are considerations in using chemotherapeutic drugs.[8,9] In this regard, nanomedicine is advantageous in posing limited side effects, high therapeutic efficacy and being biocompatible. Due to their miniature size, the nanoparticles can reach sites in which conventional therapeutics are hard to reach with enhanced solubility, effective drug release properties and biocompatibility with limited side-effects.[10,11]

Owing to the several advantages that nanomedicine poses over conventional therapeutic approaches, polymer nanoparticles are advantageous in improving the solubility and biocompatibility of drugs under trial with effective release of such drug possibilities.[12] Among the polymeric nanoparticles, natural compounds like chitosan and alginates, and synthetic polymers such as polyethylene glycol (PEG), polyvinyl alcohol (PVA) and poly lactide co-glycolic acid (PLGA) are widely used.[13] In this study, we used CNPs as they are more biodegradable, pose enhanced biocompatibility and are considered safe in being used as a part of human diet forming an integral part of wound-dressing. It is advantageous in possessing multiple routes of administration. In addition, they hold muco-adhesive properties for sustained release of the drug cargo via non-parenteral routes.[14]

CNPs are prepared using covalent crosslinking methods such as emulsification, reversed micelles, precipitation methods such as phase inversion, emulsion-droplet coalescence, crosslinking methods such as ionic gelation, electrostatic and/or hydrophobic interactions for self-assembly, deacetylation by acid hydrolysis and atomization methods such as spray drying.[15] Among these methods, CNPs prepared using ionic cross-linking have been used in treatment of several cancers[16] including liver cancer (conjugated or used as composites with agents such as doxorubicin, butyric acid, lactobionic acid, galactose and carbon nanotubes)[17–22]. They are used as a drug delivery agents for several chemotherapeutic drugs and drugs under trial including doxorubicin, 5-fluorouracil and plant-based products such as triptolide, honokiol, α-hederin, hydroxycamptothecin, piceatannol and nucleic acids. Also, the CNPs have an added advantage of being conjugated with liver-targeting agents like galactose, glycyrrhizin, folate and biotin.[23,24] These drug-modified chitosan are administered through enteral, parenteral, ocular, transdermal, subcutaneous and nasal delivery routes for localized administration with limited systemic adverse effects.[25] After drug loading on CNPs, the cargo are usually released into cancer cells based on their response to various stimuli such as pH, redox activity, ultrasound energy, light, temperature and magnetic field.[26]

As a flavonol, rutin is a glycoside found in several plants including buckwheat, tea, and apple and possesses several medicinal benefits including pharmacological activities like antioxidant, anticancer and can act as cytoprotectant, vasoprotectant, neuroprotectant and cardioprotectant.[27] In China, buckwheat rich in rutin is consumed largely in noodles and soft drinks as a health supplement which can make the arteries and veins strong and improve circulation by acting as a blood thinner.[28,29] It has been known to pose limited side-effects and possess anti-proliferative or cytotoxic potential

against a variety of cancer cells in vitro besides the antitumor effects in vivo involving cell-killing modes such as apoptosis and autophagy.[30]

Although rutin has several biological properties, the flavonoid glycoside prepared or encapsulated in nanoformulations are more soluble in aqueous media than their free forms as rutin in free form is hydrophobic with low bioavailability. Therefore, nanoformulation of rutin makes them ideal candidates for cancer therapy with enhanced therapeutic efficacy, improved solubility and bioavailability, increased gastrointestinal absorption and limited side-effects.[31–33]

The positive charge of chitosan enhances their attachment with cells thereby increasing their cellular uptake. An electrostatic attraction between negatively charged rutin and positively charged CNPs can result in an improved drug uptake, although rutin has poor loading efficacy on nanoparticles (to almost 10%), especially polymers.[34–36] The major limitations associated with the use of this plant active are that they pose neurotoxic and cardiotoxic side-effects, including the formation of hemorrhoids.[37] Hence, the nanoformulation of rutin was attempted in our report using CNPs for efficient drug delivery towards Hep3B cells, in an attempt to improve the specific targeting of cancer cells with limited toxicity. Although reports of rutin loaded on CNPs have been published,[38–40] the bioactive has been studied very little in applications related to medicine, especially cancer. They have been tested for their anticancer potential against breast and pancreatic cancer,[41,42] management of cerebral ischemia[43] with anti-inflammatory,[44] antibacterial, antioxidant, and photocatalytic activities[45] and had been suggested for possible use in cosmetics and wound healing.[46,47]

Although there are very limited reports on the use of rutin-loaded CNPs for cancer therapy, rutin has been successfully loaded on several other nanoparticles including mineral-, lipid-, ionic-liquid, silica-, PEGylated nanoliposome-, solid lipid-, nanoemulsion-, nanocrystal-, keratin-, PLGA-, platinum and palladium-based nanomaterials and on phyto-sterosomes for the treatment of breast,[48–50] lung,[51,52] renal,[53] head and neck,[54] colorectal,[31,55] cervical,[56] brain[57] and liver[58,59] cancers at the preclinical level. Other than cytotoxic effects on cancer cells, rutin conjugated with mesoporous silica, nanolipids, nanomagnesia, selenium, PLGA nanoparticles and prepared in the form of nanocrystals have been proven effective for antibacterial,[60,61] antioxidant,[62] photoprotective,[63] anti-epilectic[64] and anti-parasitic[65] activities.

These reports suggest that rutin loaded CNPs are a very less studied nanoformulation in cancer therapy, especially those of liver, which may require a lot of attention. As per published literature, there is not a single report for the use of a simple process towards the preparation of rutin-conjugated CNPs for cytotoxic effects on liver cancer cells. Although there has been a published report of rutin-loaded on chitosan-alginate nanoparticle combination tested for anti-diabetic and cytotoxic effects on HepG2 cells, it involved a dual polymer combination.[66] Hence, a simple process involving minimal reactants (no other capping agents) by loading rutin as a single therapeutic agent on CNPs was adopted and tested for their anticancer potential on Hep3B hepatoma cells, which makes it a novel and the first of its kind report internationally. According to the authors, rutin loaded on CNPs has not been tested as a single therapeutic agent for its anticancer effects on liver cancer cells. Therefore, we decided to synthesize CNPs with rutin load and test its efficacy on Hep3B hepatoma cells through a mechanistic approach for the very first time.

The hypothesis of our study was that CNPs could load rutin effectively and the rCNPs may deliver rutin successfully to the targeted pediatric hepatocellular carcinoma Hep3B cells. In this regard, the safety of the rCNPs would be tested against L929 fibroblasts, since it is believed that effective drug delivery systems are safe towards normal cells and can specifically target the cancerous cells. In addition, the hemocompatibility can provide insights into their safety in vivo and help in determining the route of administration. In addition, the mean particle size was expected to be less than 200 nm which can enter the tumor environment better than larger sized particles. Also, we expect the ROS levels to be elevated after rutin is being delivered, which could possibly cause significant changes in ULK1 and NF-κB signaling, promote autophagy and inhibit EMT, thereby preventing metastasis of Hep3B cells. Considering this hypothesis, the novelty of the study was based on the fact that the rCNPs will possess cytotoxic effects on Hep3B cells and the probable mechanism for their cytotoxic effects on the hepatoma cells could be depicted as an international report for the first time. Therefore, we attempt to follow a simple process for synthesis of rCNPs, analyze their physicochemical properties, quantify the rutin load and rutin release, assess their cytotoxic potential on Hep3B cells and determine the possible mechanism besides elucidating the safety and biocompatibility of the rCNPs. We intend to provide these insights into the use of rCNPs for therapy of liver cancer through the current research work.

Materials and Methods

All chemicals used for the research were of analytical grade, purchased from Sigma Aldrich Chemicals Co. LLC. (St. Louis, MO) and were not processed further before use for synthesis. Chitosan was bought with a degree of deacetylation of 85% (medium molecular weight) and a viscosity of 200–800 cP, 1 wt. % in 1% acetic acid (25 °C). Sodium Tripolyphosphate Anhydrous (sTPP) (57–59% and pH 9.0–10.0), Sodium chloride (≥99.0%, pH 5.0–9.0), Rutin (95%) and Rhodamine B (≥95%) were purchased in extra pure form. All solutions were prepared with deionized water during the course of the experiment.

Preparation of Rutin Loaded CNPs

The rCNPs were synthesized following methods published previously with slight modifications.[67–69] Chitosan was prepared at the concentration of 2 mg/mL in 2% glacial acetic acid and 50 mM sodium chloride and stirred using a magnetic stirrer for 1 hr at 300 rpm. The formed solution was visibly clear and free of residues and therefore no other processes such as filtration were adopted. After 1 hr of stirring, rutin was added at 2 mg/mL and 5 mg/mL (individually) and stirred for 1 more hour. This mode of adding a drug to the chitosan solution before adding the negatively charged crosslinker TPP has been reported previously.[70–72] The addition of the drug is done before addition of TPP which can help the incorporation of the drug into the chitosan matrix.[73–76] The CNPs were reported to be formed instantaneously as soon as TPP was added to chitosan solution containing a drug.[34,77] Therefore, sTPP at 2 mg/mL concentration was added after rutin has been added, for better integration of rutin into the chitosan matrix before the CNPs could be formed by crosslinking with TPP. This final solution was stirred for 1 more hour before centrifugation. The pH of the so-formed solution after the final incubation of 1 hr was 5.5 which is widely preferred and observed during the synthesis of CNPs.[78–80] The final pellet with rCNPs was obtained after centrifuging the solution at 10,000 rpm for 15 mins at 4° C. The pellet was washed by centrifugation at 10,000 rpm for three times (15 mins each time) and resuspended in normal saline every time to remove unentrapped or free drug.[81–83] In addition, the final pellet obtained after the total 1 hour of centrifugation (4 times of 15 mins) was filtered using 0.45 and 0.22 micron filters and used for further experiments. This filtration may also aid in removal of any unwanted impurities, residues or unentrapped drug.[84–87] The same procedure was followed for preparation of CNPs without any drug load (pCNPs).

Physicochemical Properties of the CNPs

Characterization of the CNPs

UV–vis analysis was conducted using Spectramax 190 absorbance reader. The surface properties of the rCNPs were studied using Perkin Elmer Spectrum RX1 model FTIR instrument. Particle size and PDI were analysed via dynamic light scattering (Particulate Systems model Nano Plus instrument). ζ-potential was analysed using Zetasizer Nano ZS instrument (Malvern Panalytical, Malvern, UK). The morphology of the synthesized CNPs was measured using JEM-2100 Plus instrument, JEOL Ltd., Japan.

Encapsulation and Drug Loading Efficacy

To begin with, the λ-max value of rutin was determined using UV–vis spectrophotometry to be 352 nm. The synthesis was conducted as mentioned earlier and the quantity of unconjugated rutin was calculated from the supernatant by analysing its absorbance at 352 nm. The calibration curve was derived to determine the concentration of rutin. The encapsulation efficiency and percentage of drug load were determined using the following formulae:[88,89]

$$\text{Encapsulation efficiency (EE\%)} = (\text{Amount of drug incorporated}) - (\text{Amount of free drug})/(\text{Amount of drug incorporated}) \times 100$$

$$\text{Drug loading \% (DL \%)} = \text{Total amount of drug incorporated in the nanoparticles}/\text{Total weight of nanoparticles} \times 100$$

Drug Release Assay

The in vitro drug release assay was conducted using dialysis membrane sacs. The procedure for preparing the rCNPs was followed as the same before using 1 mg/mL rutin as the drug and normal saline as the medium. The pellet and supernatant were collected individually after centrifugation. The supernatant absorbance was measured at 352 nm and

used for drug loading assay as mentioned earlier. The final pellet was packed in the dialysis sacs, placed into a beaker containing the dialysis medium and stirred constantly (180 rpm, 37 °C). The supernatant was collected at varying durations till the end of the 24th hr for pH 5.5 and till 102 hrs for pH 7.4 (pH adjusted with NaOH). The absorbance values were recorded and replaced with the same medium after making each reading. The differences were calculated, calibration curves were drawn, and the drug release was determined.[90] The release of rutin from rCNPs was observed at two different pH (the physiological pH 7.4 and the cancerous pH 5.5). The following formula was used for measuring the percentage of drug release:

$$\text{Drug release}\,(\%) = \text{Released drug}/\text{Total drug} \times 100$$

Quantification of Rutin Load on rCNPs Using UPLC

An UPLC method of run to determine the rutin concentration was performed using WATERS ACQUITY UPLC H-Class System. The analysis was performed using water-acetonitrile gradient elution (as a mobile phase), using a PDA detector, the column compartment temperature was 35 °C, and the samples were analyzed using multi-wavelength detectors (100 to 450 nm) and the results were quantified at 280 nm. The flow rate was maintained at 1 mL/minute. The total run time of this analysis was 30 mins. The initial conditions for gradient elution were 2.0% of eluent B with gradual increase of linear gradient to 15.0% starting at 0.01 to 7.0 minutes, followed by linear gradient to 20.0% eluent B at 15 mins. Further, the linear gradient was set at 20.0% of eluent B was set for 20 mins, 35.0% of eluent B at 25.0 mins and 10.0% of eluent B at 28.0 mins. The mobile-phase composition returned to the initial condition at 30.0 mins.

Cytotoxic Effects of CNPs on Cancerous Hep3B and Normal L929 Fibroblasts

All cell lines used in this study were purchased commercially from the American Type Culture Collection (ATCC, Manassas, VA, USA). Human hepatoma cell line Hep3B (ATCC® HB-8064™) was cultured using Dulbecco's Modified Eagle Medium (DMEM) at 1×10^4 cells per well and provided with 1X Antibiotic Antimycotic solution in addition to 10% fetal bovine serum and incubated for 24 hrs at 37 °C with 5% CO_2. Later, the cells were treated with various concentrations of the pCNPs and rCNPs. After aspirating the medium, the cells were treated with 0.5 mg/mL MTT and incubated at 37 °C for 4 hrs. At the end of incubation period, the dye was discarded. The resultant cells were analyzed using a microplate reader at 570 nm. The safety of the rCNPs was analyzed using the same protocol with an alternative normal fibroblast cell-line L929 (ATCC® CCL-1™) in place of Hep3B cells. The protocol remained the same except the cell line.[91] The experiments were conducted in triplicate, and the data were recorded as mean ± SEM.

Mechanistic Analyses for Cytotoxic Effects of rCNPs on Hep3B Cells

Evaluation of Changes in Mitochondrial Membrane Potential (MMP) and Reactive Oxygen Species (ROS)

The Hep3B cells were adhered at 2×10^5 cells per well overnight and treated with the rCNPs and incubated for 8 hrs to determine the mitochondrial membrane potential (MMP). After incubating, the cells were treated with rhodamine 123 at 1 µg/mL for 30 mins at 37 °C. The treated cells were subsequently washed and observed using a Nikon ECLIPSE TE2000-U fluorescent microscope. The average fluorescence was measured and elucidated using a bar graph.[92,93] Similarly, 5×10^5 cells were adhered overnight, treated with the rCNPs and incubated for 8 hrs to determine the intracellular ROS. At this stage, the media was removed, 5 µM H2DCFDA was added, incubated for 30 mins at 37 °C and observed using a fluorescent microscope.[94]

Analysis of Gene Expressions Using qPCR

The Hep3B cells were plated in 96-well plates at a concentration of 1×10^4 cells per well in DMEM media. The media was supplemented with 1X Antibiotic Antimycotic Solution and 10% fetal bovine serum. The optimal conditions of 37°C and 5% CO_2 were maintained for cell growth. The cells were later treated with rCNPs for 24 hrs at conditions of 5% CO_2 and 37°C. The cells were collected, washed with PBS and used for extracting RNA using standard protocols. For gene expression studies, reverse transcription was performed using PrimeScript™ cDNA Synthesis Kit. Reverse transcription reactions were confined to 3 µg of total RNA samples, 1 µL of Oligo dT Primer (50 µM), 1 µL of dNTP Mixture (10 mM each), 4 µL of 5X

PrimeScript Buffer, 0.5 µL of RNase Inhibitor (40 U/µL), and 1 µL of PrimeScript RTase (200 U/µL) and were topped off to 20 µL with DEPC treated water. The incubation for reverse transcription was maintained at 42 °C for 60 mins, and termination of the reaction was done at 95 °C at 5 mins. The reaction volume consisted of 25 µL, including 12.5 µL of 2 × AccuPower® 2X Greenstar™ qPCR Master Mix, 10 µmol forward/reverse primers, and the cDNA samples. The amplification protocol contained of denaturation at 95 °C for 15 mins, followed by 40 cycles at 95 °C for 15s and 60 °C for 30s. β-actin was used as an internal control. The results were expressed as relative gene expression using 2(-Delta Delta C(T)) method.[95] The list of primers used for the study is presented in Supplementary Table 1.

Cellular Uptake and Internalization of rCNPs

The rhodamine B-rCNPs conjugate was prepared at the ratio of 4:1 and kept for 24 hrs under dark conditions. Hep3B cells were seeded in 24-well cell culture plates, and the culture conditions were followed as that of the one followed for analysing the cytotoxic effects (cultured under standard optimal conditions of 37 °C and 5% CO_2). After a confluence of 80% was reached, the cells were treated with rhodamine B-rCNPs conjugate for 24 hrs. At the end of the treatment, the cells were washed three times with 1X PBS. Later, the treated cells were observed under a fluorescent microscope [EVOS™ FLoid™ Imaging Station] using red filter, and the images were presented at 125 µm.[96,97] The same procedure was followed for quantification of uptake, yet, at the end of treatment the cells were analyzed by a fluorescence spectrophotometer (Lionheart FX automated microscope, BioTek) using an excitation wavelength of 555 nm and emission wavelength of 627 nm.

Hemocompatibility of rCNPs

Blood collection for hemocompatibility assay[98] from healthy volunteers (n = 6) was authorized by The First People's Hospital of Changzhou Research Ethics Committee (number: 2023–076). The experiment was undertaken with the understanding and written consent of each subject. The collected blood was mixed into a heparin-coated vacutainer tube and diluted with PBS (pH 7.2, 1:9 v/v). Aliquots of 1 mL were prepared and different concentrations of the rCNPs were added to the tubes. Considering Triton X as the standard, the tubes were incubated at 37 °C. After 24 hrs, the samples were centrifuged at 3000 rpm for 10 mins, the supernatant was collected and quantified at 545 nm using a spectrophotometer. The percentage of hemolysis was calculated using the following formula:

$$\text{Hemolysis}\,(\%) = [\text{OD of drug} - \text{treated}/\text{OD of positive control}] \times 100$$

Statistical Analyses

All experiments were conducted in triplicate, and the intergroup differences were determined by Student's *T*-test using GraphPad Prism 5 software. The data are presented as mean ± standard error of mean (SEM). A p-value was deemed to be statistically significant (* $p > 0.05$, ** $p < 0.01$ and *** $p < 0.001$ for cell culture assays, ** $p < 0.05$, *** $p < 0.001$ for qPCR and *** $p > 0.001$ for other experiments).

Results and Discussion

Characterization and Identification of Drug-Loading Onto CNPs

UV–Vis Analysis

Initially, the CNPs were characterized by using UV–vis analysis. The pCNPs showed highly dominant characteristic peaks for CNPs at 305 nm. The peaks at this range are characteristic for CNPs.[99,100] Nonetheless, the loss of 300 nm peak and the occurrence of a dominant peak at 335 nm, 355 nm and 375 nm are characteristic for the synthesis of CNPs in unfiltered samples, as peaks around 360 nm relate to drug-loaded (as peaks around 360 nm is characteristic for λmax values of rutin) rCNPs. These peaks identified for rCNPs correspond well to UV–vis peaks for CNPs loaded with rutin as the characteristic peak for rutin stays around 360 nm.[101–103] The shift in peaks from their initial wavelength observed around 300 nm could be attributed to the encapsulation with a drug (rutin in this case).[104] The outcomes of UV–vis analysis initially signify that rutin has been possibly loaded onto the synthesized rCNPs. The UV–vis peak for pCNPs corresponds to 305 nm which confirms the synthesis of pCNPs without any drug interference as described above. The

peaks observed at 335, 355 and 375 nm is characteristic for rutin loading on rCNPs. The peaks around 360 nm have been reported to be the characteristic range and a standard for identifying rutin load on nanoparticles (Figure 1).[105,106] The formation of CNPs loaded with rutin implying deacetylated chitosan was achieved by ionic gelation through dipole ionic and electrostatic interactions between nitrogen phosphorus groups of compounds. A competition between phosphate and hydroxyl groups for interacting with deacetylated chitosan can occur. Therefore, deprotonation of deacetylated chitosan can be formed by hydroxyl groups, and a greenish milky suspension (green tint of rutin) was produced as a result of such interactions between deacetylated chitosan and rutin under stirring.[107]

FTIR Analysis

The FTIR peaks around 3440 cm^{-1}, 1638 cm^{-1} correspond to the broadening vibrations for chitosan. These peaks related to CNPs are due to the reactivity of amine groups which can interact with phosphate groups of sTPP. Also, the peak at 2080 cm^{-1} is related to the alkyne or carboxylated amine groups attributed to the CNPs.[108–110] In addition, the shift in peaks from pCNPs from 1455 cm^{-1}, 1364 cm^{-1}, 1294 cm^{-1}, 1205 cm^{-1}, 1095 cm^{-1}, 1015 cm^{-1} and 560 cm^{-1} to 700 cm^{-1} (0.45 micron filter) and 665 cm^{-1} (0.22 micron filter) in the rCNPs could be related to electrostatic interaction between rutin and chitosan and the consequent grafting[111,112] (Figure 2). This interface is a common occurrence as an outcome of interaction between the drug and the nanomaterial and therefore the entrapping of rutin had occurred on the rCNPs.[113] The disappearance of FTIR peaks indicates that a strong chemical interaction has occurred between the drug and the polymer nanoparticles.[114] Some peaks do shift from their original value and some peaks remain the same even after the formation of the polymeric nanoparticles after the drug load in CNPs.[115] This was the case with our study as several peaks disappeared in the rCNPs in comparison to the pCNPs. Also, some peaks remained in both pCNPs and rCNPs (three peaks around 1634 cm^{-1}, 2080 cm^{-1} and 3440 cm^{-1}). This indicates that a strong interaction has occurred between rutin and chitosan resulting in the formation of

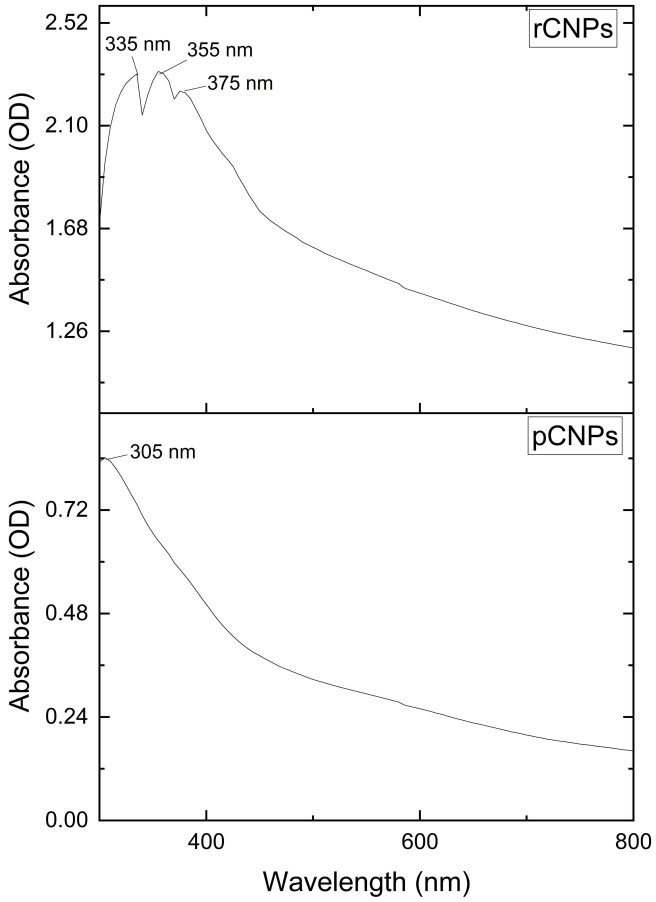

Figure 1 UV–Vis analysis of the rCNPs and pCNPs.

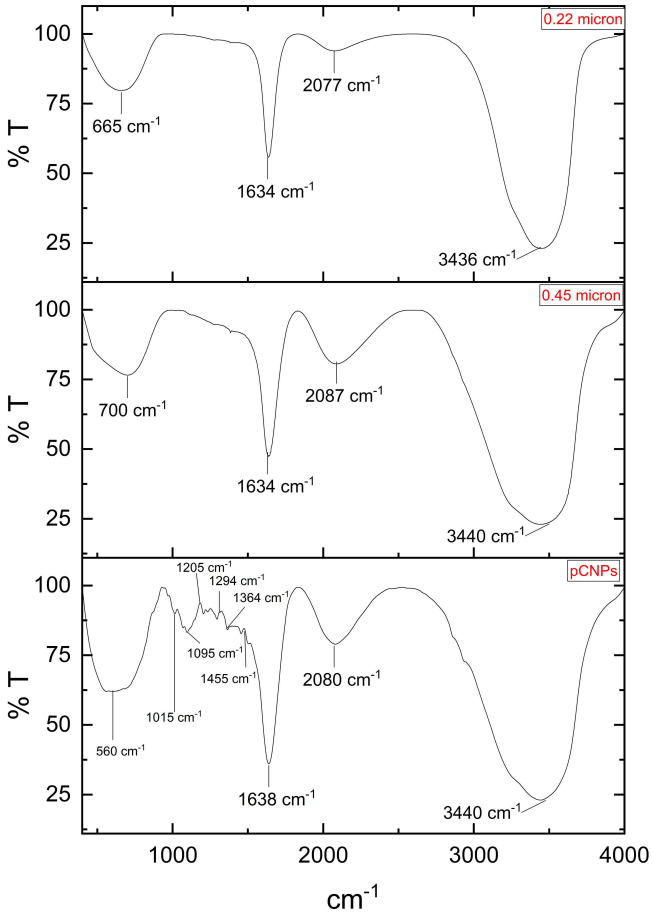

Figure 2 FTIR analysis of the pCNPs, 0.45 micron filtered rCNPs and 0.22 micron filtered rCNPs.

rCNPs. This is a secondary illustration for loading of rutin on rCNPs. For further confirmation of the loading of rutin onto rCNPs, we performed an UPLC analysis, which may also provide the information on the volume of rutin loaded on rCNPs.

Determination of Drug Load by Using UPLC

Liquid chromatography is one of the most preferred methods for determination of rutin using a PDA detector as it is efficient for quantitative analysis of compounds loaded on nanomaterials for their advantages with accurate and precise detection and/or quantification.[116] In comparison to UV–vis which determines the results in two aspects such as light intensity and time, PDA-based detection complements the outcomes through a third aspect with respect to wavelength.[117] Among liquid chromatographic techniques, UPLC has several advantages as it needs the sample in small volumes, shorter run times with decreased use of solvents and therefore is an economical method for rapid quantification of biomedical agents.[118] With this rationale, the data retrieved by UPLC was used in determining the quantitative load of rutin on rCNPs. In this regard, the retention time of standard rutin was 18.735 min; comparatively, the retention time for 0.22 micron filtered samples was 19.077 min (Supplementary Figure 1A and B). Thus, UPLC analysis was the third assay to confirm that the synthesized rCNPs were loaded with rutin and the concentration was quantitatively measured after filtration with 0.22 micron filter to be 88 µg/mL. Therefore, UPLC remained an assay for both identification of rutin load and quantification of its concentration in the rCNPs as per our study.

Particle Size, PDI, Zeta Potential and Morphology

After the initial analyses of the loading of rutin on to CNPs as rCNPs using UV–vis, FTIR and UPLC, the average particle sizes and PDI were determined for all three samples prepared at the initial rutin concentration of 2 mg/mL during synthesis (unfiltered, 0.22 micron and 0.45 micron filtered samples). Since these two measures are important for

determining the superiority of the particles, they were analyzed.[119] The particle sizes for the unfiltered pCNPs and rCNPs were 924.7 nm and 827 nm, respectively. Subsequently, the PDI were 0.515 and 0.466 for the samples. The particle sizes for 0.45 micron filtered pCNPs and rCNPs were 195.8 nm and 207.4 nm, respectively, whereas the PDI were 0.313 and 0.308. Similarly, the particle sizes for 0.22 micron filtered pCNPs and rCNPs were 147.7 nm and 140.0 nm, respectively. Accordingly, the PDI were 0.243 and 0.226.

Similarly, the initial drug concentration set at 5 mg/mL for rCNPs showed particle sizes of 112.2 nm, 113.1 nm and 144.1 nm for unfiltered, 0.45 micron and 0.22 micron filtered samples. The PDI values were 0.297, 0.307 and 0.244, respectively (Figure 3A). Since the cytotoxic effects were prominent in 0.22 micron filtered samples of 5 mg/mL rutin precursor (which is presented in the following section), it was used for further biological assays (144.1 nm size and PDI of 0.244). The particle size observed in this study was similar or very small to those of nanoparticles loaded with rutin that had been published previously (~50 to 200 nm or even up to 7.8 µm). Also, in those reports, the PDI stayed in the zone of 0.2 to 0.4, similar to our study.[120–123]

According to the proposed Gaussian distribution, particles of the nano-size which possess a PDI range of 0.1 to 0.4 are presumed to reflect moderate polydispersity.[124,125] Also, the particle sizes of less than 200 nm can extravasate into the tumor

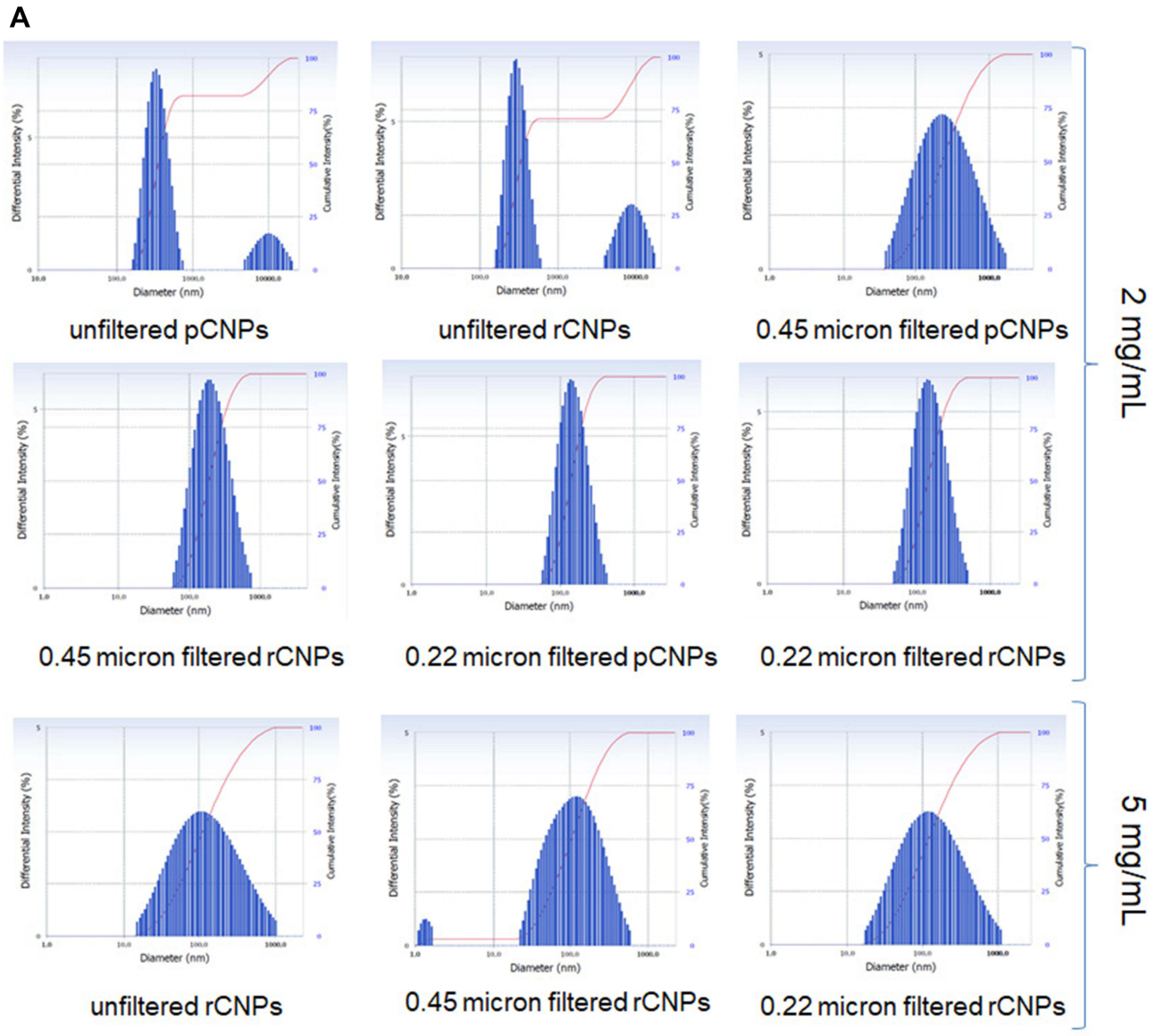

Figure 3 Continued.

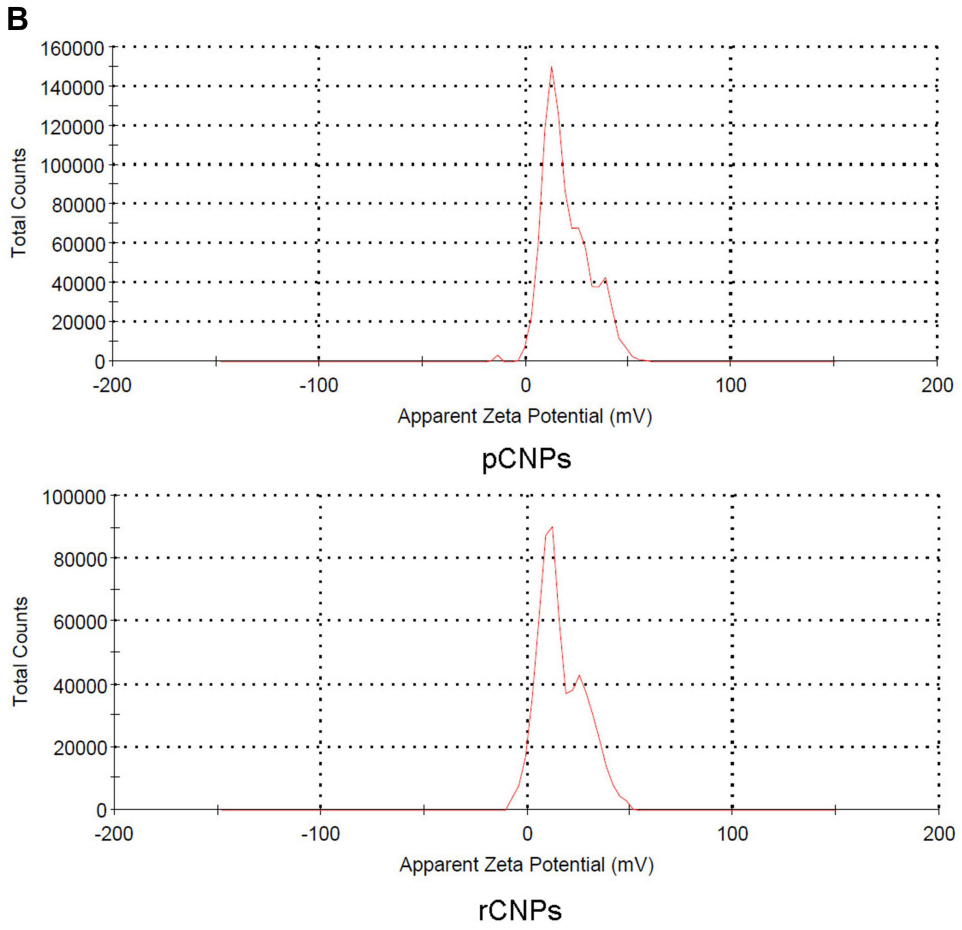

Figure 3 (**A**) Particle size analysis for the initial drug concentration set at 2 mg/mL for pCNPs and rCNPs along with the initial drug concentration set at 5 mg/mL for rCNPs. (**B**) Zeta potential of pCNPs and rCNPs.

environment with a width of 400 to 600 nm via enhanced permeability and retention (EPR) effect.[126–130] Since, the rCNPs were within the size range of 200 nm (144.1 nm) and possessed a PDI of 0.244, they seem ideal for tumor targeting.

ζ-potential is widely accepted as an electrokinetic indicator for the stability of a colloidal solution, which determines the electrostatic repulsion between similarly charged nanoparticles in a colloidal suspension. Higher ζ-potential index of the nanoparticles elucidates that the solution is exceedingly stable and the particles can repel each other and stay unaggregated. When the ζ-potential value is low, the particles in the solution are determined to possess limited stability, repel less or attract more, leading to colloidal breakage and flocculation or aggregation.[131] ζ-potential values ranging between −10 mV and +10 mV are considered neutral, whereas values higher than −30 mV and +30 mV are extremely stable as anionic and cationic forms, respectively.[132] The ζ-potential value of pCNPs was 19.7 mV, whereas that of rCNPs was 16.4 mV, indicating good stability (Figure 3B). Particles with ζ-potential of around 20 mV are considered stable and possess very low probability for aggregation.[133] It is also interesting to note that positively charged CNPs pose enhanced rapid and greater cellular uptake.[134] In addition, drug loading on CNPs can result in decrease of ζ-potential as observed in this case and previous reports. The decrease in the value could also be attributed to the charge of the drugs loaded on the polymer (negative charge of rutin in this case).[135–138] The decrease in ζ-potential after drug load could be due to the encapsulation of the drug inside a polymer complex, rather than adsorption on its surface. In addition, a moderate and positive ζ-potential can improve the circulation time of the drug in the blood.[139] Hence, the ζ-potential of rCNPs indicates that they can deliver rutin with better circulation time, enhanced stability and improved cellular uptake.

To study the morphology of the synthesized rCNPs, TEM analysis was adopted. Particles at the nano-regime are generally observed at different magnifications using TEM.[140] The TEM observations for rCNPs, the histogram for determination of their particle size and the observations for pCNPs are provided in Figure 4. The mean particle size

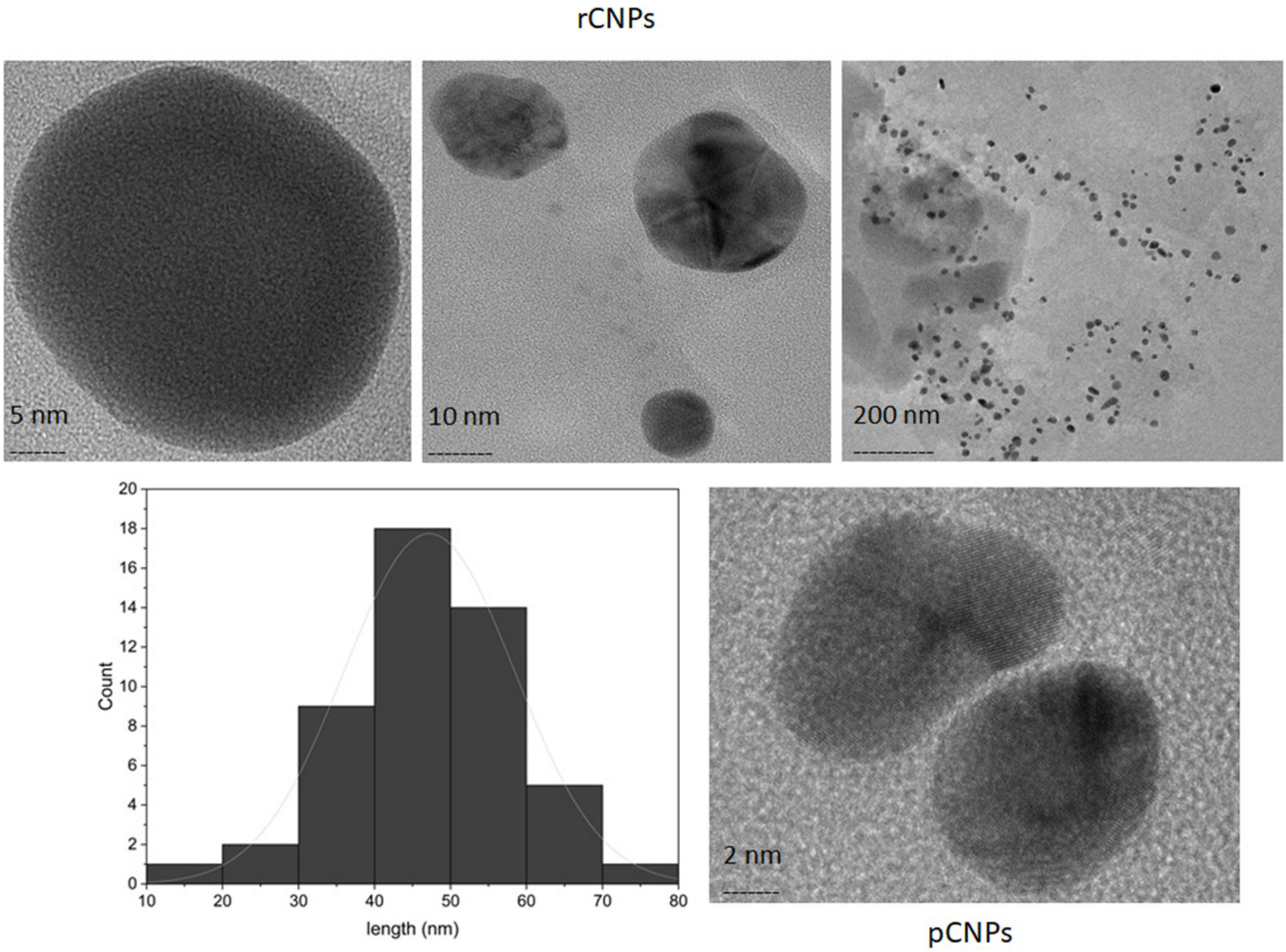

Figure 4 Morphology (5, 10 and 200 nm) and the histogram for particle size of rCNPs along with the morphology of pCNPs (2 nm) using TEM.

calculated using TEM was 47.208 nm. As per the outcomes, the comparison of particle sizes using DLS and TEM indicated that the particle sizes according to DLS (144.1 nm) were higher than TEM (47.208). This is because TEM is a local analysis of the materials, whereas DLS is a holistic or wide-area analysis of the concentration of the light being disseminated round the zone that is being investigated. Hence, DLS is a much preferred method for materials being used in solvent forms containing biological agents.[141]

In vitro Drug Loading and Release

After the physicochemical properties of the rCNPs were determined, DL % of the rCNPs was calculated and found to be 13.29 ± 0.68%, whereas the EE % was 19.55 ± 1.01%. The hydrophobic nature of rutin makes it a drug, with low loading efficacy (around 10%) on several polymeric nanoparticles as is commonly observed among other hydrophobic drugs and nanomaterials. Suggestively, the DL% observed in the present study for rutin on chitosan was comparatively higher (compared to the previously reported 1.9 to 4.6%) or almost similar (below 10% widely observed for polymeric nanoparticles) to the percentage reported by previous publications.[136,142–144]

UV–vis is a rapid, inexpensive, easy and reliable method which meets the necessities of quality control in pharmaceutical standards and is therefore effective for examining the drug release using a polymer system.[145,146] It is advantageous for determination of drug release in comparison to HPLC as there is a hindrance in continuous monitoring of drug release from nanomaterials. The UV–vis method is therefore a highly sensitive and comfortable method for estimating the drug release.[147] With regard to determination of drug load, both methods can comparatively provide the information of drug load, and it is better to use both methods in unison. Yet, liquid chromatography is a more precise

method compared to the use of UV–vis for serving this purpose. In addition, concentration detection using both UV–vis and liquid chromatography may have differences of up to 6 fold (UV–vis showing higher values than liquid chromatography). Relating to this, as per UV–vis analysis, the drug loading capacity was around 13.29 ± 0.68%, which is approximately equivalent to around 133 µg/mL, whereas, the drug load on the rCNPs calculated using UPLC was 88 µg/mL (The concentration calculated using UV–vis was 1.5 fold higher than concentration calculated using UPLC as per our study). Hence, liquid chromatography is more effective in quantification of a drug compared to UV–vis.[148,149] Therefore, we used the drug concentration calculated using HPLC to determine the dose for all our cytotoxicity and related experiments, whereas, considered UV–vis with regard to drug release for its advantages of continuous monitoring.

Considering the advantages of UV–vis over liquid chromatography, the release profile of rutin was observed using UV–vis till a time period of 24 hrs at the cancerous pH 5.5. The release was not evident until 15 hrs, the point from which there was a burst of rutin release starting from 18 hrs. The burst release happened till 24 hrs, at which duration, 88.58% of the drug was released. This similar pattern of rapid release of similar concentration of a drug over a definite period of 24 hrs has been reported previously.[66,150] Contrastingly, a slow and sustained release was at the physiological blood pH of 7.4. The drug release was not observed until ~ 70 hrs, while, at 72 hrs, the drug release was ~2%. A sustained release was observed thereafter which reached 91.44% after 102 hrs (Figure 5). The drug release at pH 5.5

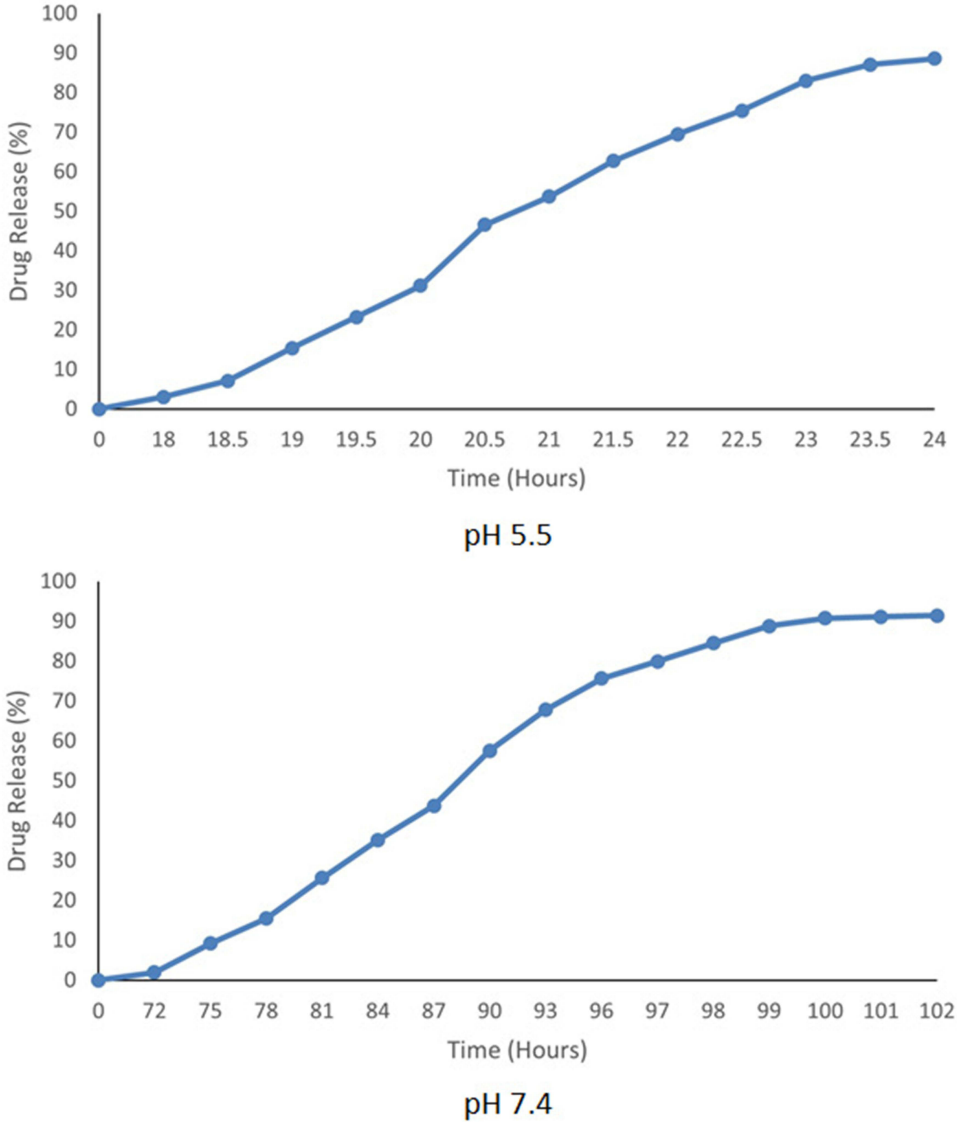

Figure 5 In vitro drug release of rutin at cancerous pH 5.5 and physiological pH 7.4.

was 4.25% faster than the release at pH 7.4. This pattern of difference in release has been reported previously where the release at pH 7.4 is much slower than the release at acidic pH (from 2 to even 20 times slower).[151–153] The data for percentage of drug release at different time intervals are provided in Supplementary Table 2A and B.

As per previous reports, pH 5.5 is the intracellular pH displayed by cancer cells, especially, in liver cancer,[154–158] and also represents the lysosomal pH.[159,160] However, pH 7.4 relates to normal physiological pH.[161,162] The enhanced release of rutin from rCNPs at pH 5.5 compared to pH 7.4, which could accumulate more at lysosomal or cancerous pH of Hep3B cells, might be attributed to several factors and outcomes including: 1. Swelling property and high permeability of CNPs at acidic pH atmosphere results in a drug release which was maintained mutually owing to both erosion and diffusion;[163,164] 2. The hydrolysis of the bonds within cationic hydrophilic polymers such as chitosan that are sensitive and labile to the acidic pH;[165] 3. In the diffusion-controlled release, a rapid release is achieved initially as drug molecules are evenly distributed in the polymer matrix which can absorb the surrounding aqueous medium, expand and diffuse later resulting in an osmotic release;[166] 4. At the lysosomal pH of cancer cells which stays around 5.5,[167] the proton sponge effect occurs, as the accumulation of positively charged molecules in the form of polymers such as chitosan disrupt the lysosomes due to influx of chloride ions and result in efficient drug delivery after escaping endosomal degradation.[157] As soon as the CNPs infiltrate the cancer cell membrane by endocytosis and escape lysosomal degradation, they enter the nucleus and bind with the DNA and lead to its aggregation or the subsequent genotoxic effects;[168,169] 5. The positive charge of CNPs facilitates effective attachment to cancer cells, thereby resulting in increased cellular uptake and eventual drug release;[134] 6. Reduction of electrostatic interfaces taking down the nanovalves with the cargo resulting in increased release of the drug as a result of protonation of amines below pH 7.[170] Therefore, drugs with rapid or enhanced release at pH 5.5 could possibly lead to superior therapeutic efficacy in vivo.[171] Such pH-responsive materials can therefore be stable at physiological pH of the blood and breakdown (due to changes in the degree of ionization) to release the drug cargo under acidic environment.[172] This could be the rationale for the enhanced drug release at pH 5.5 as observed in our study.

The drug release may also be affected by factors such as drug composition, mode of preparation, interactions between drug and the polymer, and the release mechanism may involve the diffusion of drug molecules or by polymer matrix degradation.[166,173] The sustained release is advantageous for every day dosing in clinical patients in preventing the reversal of drug-effect and reduction of frequency of dosing.[174] Since accumulation of the antitumor drug within a tumour is preferred in comparison to the normal cells, nanomaterial-based drug delivery is desired. In such cases of using pH-responsive nanomaterials, the release is multi-fold better at pH 5.5 than 7.4, which is widely preferred.[175] The drugs loaded on these pH-responsive nanomaterials are released in a rapid manner as these materials can also be degraded by the lysosomes and endosomes at acidic pH. These materials can therefore enter cancerous cells efficiently compared to normal cells. Also, the toxic effects on cancerous cells were higher, whereas a low toxicity profile was exhibited on normal cells.[176,177] This might be due to the fact that the nanomaterials stay in the blood pH for prolonged durations, penetrate tissues and release the drug at the acidic pH (the one at targeted tumor location) with limited side-effects.[10] These kinds of materials which can show excellent extracellular stability (relating to pH 7) and release the drugs in a rapid manner at cancerous pH are sought for effective cancer therapy.[178] Similar properties exhibited by the rCNPs in this study may therefore be effective in tumor-targeting with limited adverse effects.

Interactions of the CNPs with Hep3B Cells and the Possible Mechanisms

Cytotoxic Effects of the pCNPs and rCNPs

Cells at the in vitro stage form the base for preclinical testing and are therefore used in identifying a drug possibility.[179,180] Since MTT assay is a distinctive standard for determining the cytotoxic effects of a drug possibility, it was adopted further.[181] After incubating the Hep3B cells with the unfiltered and 0.22 micron filtered rCNPs for 24 hrs, the cell-killing effects were elucidated by using MTT assay. The outcomes of the assay indicated that the values for inhibitory effects on Hep3B cells by 50% using unfiltered and 0.22 micron filtered rCNPs were 463.9 ± 0.07 μg/mL and 9.7 ± 0.19 μg/mL (based on the rutin load on rCNPs), respectively. The IC_{50} for the cytotoxic effects of pCNPs on Hep3B cells was 442.6 ± 0.15 μg/mL (Figure 6). The cytotoxic effects of 0.22 micron filtered rCNPs were more pronounced than rutin-free pCNPs or unfiltered rCNPs.

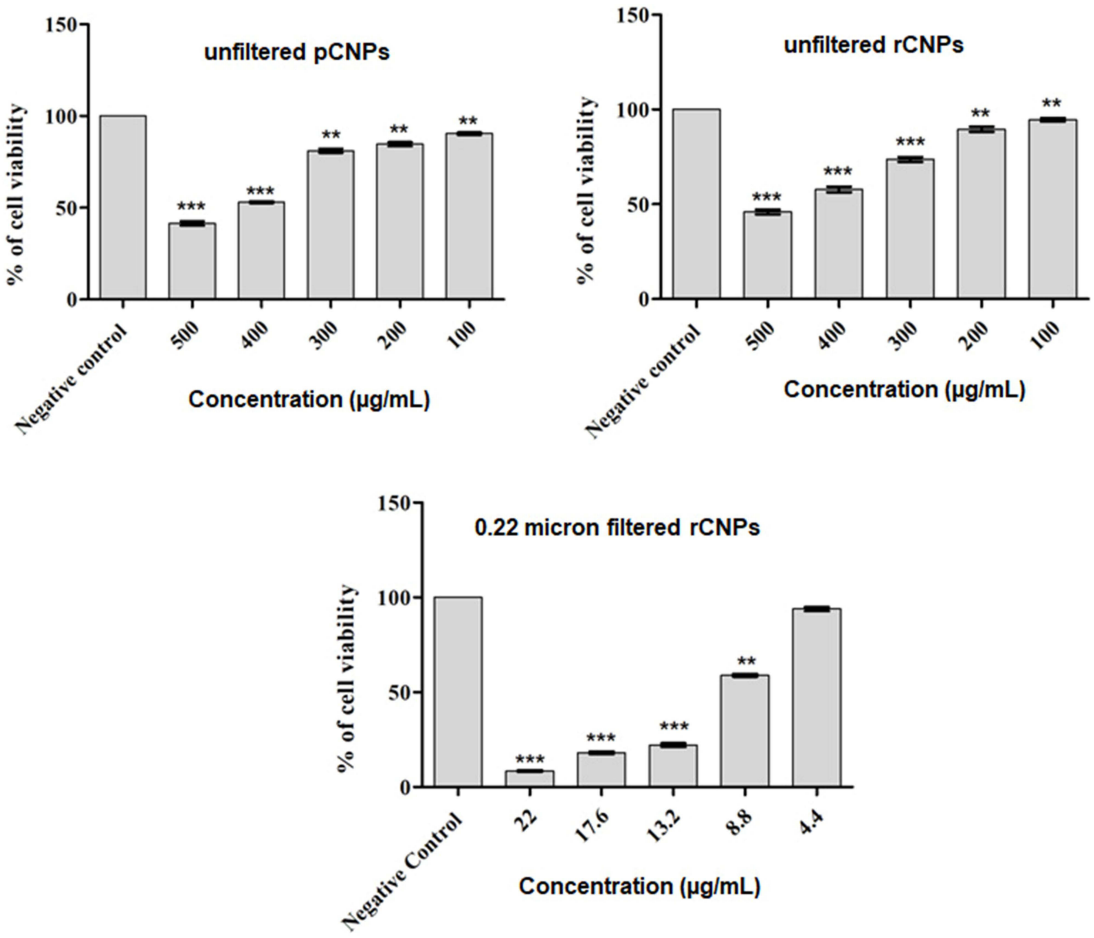

Figure 6 Cytotoxic effects of the pCNPs and rCNPs on Hep3B cells in triplicate and expressed as mean ± SD (**p < 0.01, ***p < 0.001).

Since the IC_{50} value was more significant or effectively cytotoxic after being filtered with 0.22 micron filter, it was used for further studies related to biological effects on Hep3B cells. The dose-dependent cell-killing effects were therefore effective at a lower rutin dose when filtered using a 0.22 micron filter as indicated by the IC_{50}. The microscopic observations of the interactions between the CNPs and Hep3B cells are presented in Supplementary Figure 2A and B. It has been reported that nanoparticles with no drug load (plain nanoparticles) displayed limited cytotoxic effects on cancer cells, whereas, the nanoparticles with a conjugate are more toxic to the cancer cells.[182,183] Similar results were observed in our study as pCNPs were less toxic on cancer cells in comparison to the rCNPs.

Changes in MMP and ROS

Since MMP is a widely accepted tool to display the mitochondrial function and can induce changes in production of ROS, it was analyzed further. This is based on the fact that intervening the MMP levels by therapeutic approaches can help sustain several clinical diseases by decreasing the viability of cells related to such disorders.[184–186] Since the mitochondrion is responsible for ATP production, changes in MMP can lead to changes in ATP production and the pH of mitochondrial sub-compartments.[187–189] Specifically, increased production of MMP can lead to changes in morphology of mitochondria including the intermembrane space and matrix and lead to induction of cell death via mechanisms such as apoptosis.[190] Hence, damages to the mitochondria and subsequent changes in ROS can lead to changes in metabolic processes related to energy and thereby a reduction in production of ATP.[191–193] Since increased production of ATP can lead to tumor progression, changes in MMP can affect the metabolic process of cancer cells as ATP is the primary energy source for cancer cells.[194,195] The increased production of MMP as observed in the study indicates that ATP levels could proportionately be decreased and the supply to Hep3B cells could be hindered (Figure 7). Also, the materials that can cause changes in MMP can successfully

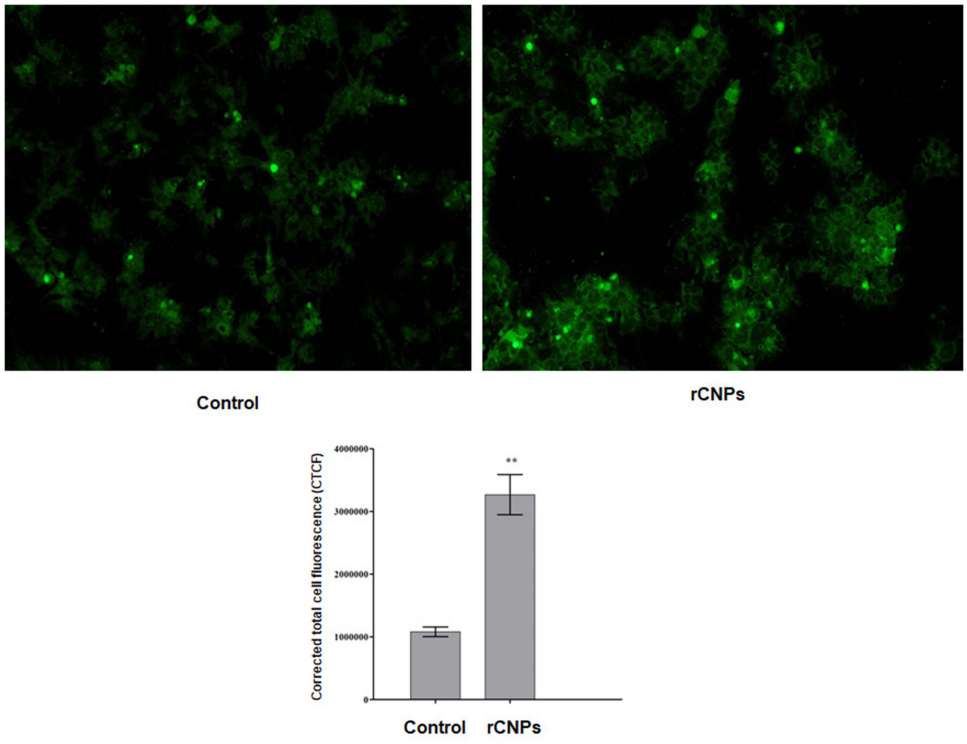

Figure 7 Changes in MMP after treating Hep3B cells with rCNPs (**p < 0.01).

target cancer cells, making them more prone to drugs that target mitochondria, the organelle which is considered the primary target for several tumor-targeting agents.[196] These changes in MMP can induce cell-killing mechanisms such as autophagy in cancer cells.[197] Therefore, rCNPs could target mitochondria and result in cell-killing mechanisms including autophagy for their therapeutic effect on Hep3B cells.

ROS production primarily occurs in the mitochondria and can cause mitochondrial damage and consequent depleted levels of ATP.[198] In this regard, increased generation of ROS can lead to increased production of MMP leading to changes in mitochondrial respiration and eventual dysfunction and the vice versa.[184,199,200] Therefore, the ROS levels after treatment with rCNPs were analyzed. In general, ROS is necessary for nanomaterials to trigger cancer cell death. The production of ROS by changes in systematic functioning of redox-dependent activities is dependent on nanomaterial characteristics such as size, contour, exterior features and characteristics like dissolution and aggregation which may decide the intensity and outcome of particle-cancer cell interactions.[201,202] At elevated levels of ROS, cancer cells undergo apoptosis as a consequence of the generation of the reactive species.[203] Such reactive species can also induce autophagy and ferroptosis which can result in cell death of malignant cells.[204,205] Elevated levels of ROS observed in this study can possibly lead to cell killing mechanisms such as NF-κB signaling and changes in ULK1 signaling (Figure 8).[206,207]

Analysis of Gene Expressions Using qPCR

qPCR is widely used to define the varied expression levels of mRNA in various cancer cell types, thereby determining the mechanisms of certain cell-killing effects which are usually determined by the expression fold as a function of upregulation or downregulation.[208–211] In this manner, the changes at the gene levels of certain key proteins can be determined which can be useful in studying the key mechanism of drug–cell interactions.[212] As mentioned earlier, by means of causing the changes in MMP and ROS, a drug candidate can possibly result in engagement of NF-κB signaling and ULK1-linked autophagy in cancer cells. Therefore, we further intended to analyse the changes in ULK1-related autophagy associated genes and NF-κB signaling.

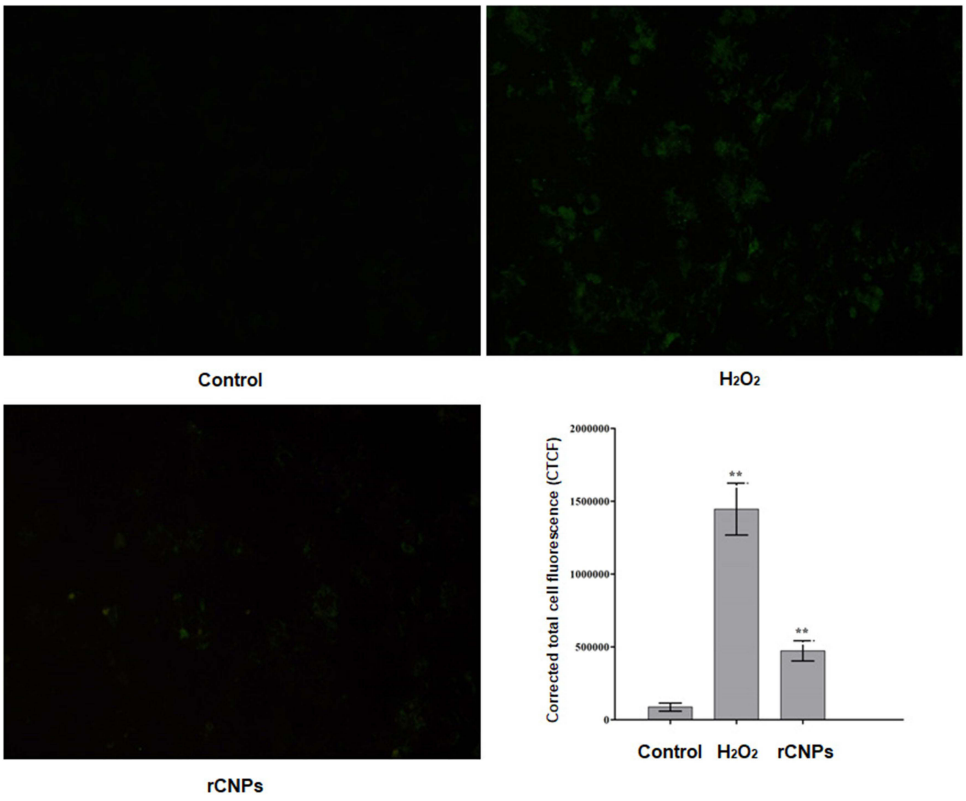

Figure 8 Changes in ROS after treating Hep3B cells with rCNPs (**p < 0.01).

Macroautophagy is a catabolic mode of cell-killing where certain regions of the cytoplasm are impounded into the membrane-bound vesicles called autophagosomes. Later, the constituents are transferred to the lysosome for degradation. This process begins with the formation of phagophore, engulfing of the cargo, elongation of the phagophore leading to the formation of autophagosome. The autophagosome binds with the vacuoles and results in the formation of autolysosome which degrades the cargo and releases them back into the cytosol.[213] In this process, ULK1 is activated by 5′ adenosine monophosphate activated protein kinase (AMPK)-dependent phosphorylation, thereby leading to the formation of ULK1 complex. Also, ROS plays a critical role in phosphorylation of ULK1 and promotion of autophagy.[214] This process of formation and/or phosphorylation of the ULK1 complex requires the roles of several autophagy-related proteins, where phosphorylated ULK1 fuses with Beclin 1 and assembles the phosphoinositide-3 kinase (PI3K) complex. The upregulation of ULK1 in this study indicates that the cell-killing mode of autophagy was initiated. This complex attaches the phosphatidylinositol lipids that can recruit the ATG proteins to result in the formation of autophagosome.[215] Relating more to this analysis of effects of ULK1 and autophagy, the upregulation of ULK1 has been associated with cell-killing of drug-resistant cancer cells via the induction of autophagy. This process may engage the involvement of autophagy-related 5 (ATG5) and LC3II for the induction of autophagy.[216–218]

Autophagy-related genes (ATGs) are critical constituents of both the canonical and non-canonical autophagy. After the formation of autophagosome, the elongation and maturation take place by the mediation of ATG5-ATG12-ATG16 complex. The upregulation of ATG5 expression in our study supports the formation of this complex and therefore the maturation of the autophagosome which is termed as the ubiquitin-like conjugation system. This supports the conjugation of LC3 with phosphatidylethanolamine which is called the lipidation conjugation system which happens with the help of ATG3. This induces the formation of autophagosome and fusion, with the lysosome leading to the formation of LC3II.[219] It is critical to note that LC3II is a marker for macroautophagy, where LC3 leads to the formation of LC3II at the membrane with an intermediary LC3-1.[220–222] The upregulation of LC3II signifies the induction of macroautophagy in this study. The cargo to be degraded is now presented to LC3II inside the autophagolysosome, where the lysosomal

secretions dissipate the cargo (the extracellular or intracellular macromolecules and organelles) by means of autophagy.[223–226] In our study, the upregulation of ULK1, ATG3, ATG5 and LC3II after treatment with rCNPs indicates that these nanomaterials induced ATG-dependent autophagy via engaging the ULK1 complex along with the involvement of LC3II. Hence, we further analyzed the role of NF-κB signaling in cell death induced by rCNPs.

NF-κB is in general considered an oncogenic transcription factor and includes a family of proteins that are usually engaged in malignant transformation and progression besides inducing EMT. Yet, in certain cancers including liver, NF-κB acts as a tumor suppressor.[227–230] Also, p53 as an established tumor suppressor can activate autophagy for the purpose of cancer cell killing.[231,232] It has also been reported that p53 and NF-κB can drive the formation of a pro-inflammatory environment which can benefit the drug possibilities in tumor therapy.[233] The upregulated expressions of p53, NF-κB1 and NF-κB2 in this study support the tumor-inhibiting roles of these protein families or their constituents on Hep3B cells since the activation of p53 and NF-κB signaling could be related to induction of autophagic cell death.[234,235] There are reports suggesting the roles of these two pathways in treatment of liver cancer along with the involvement of autophagy.[236–238] Therefore, the upregulated expressions of p53, NF-κB1 and NF-κB2 in this study could relate more to autophagy-linked cell death. There are evidences that autophagy can prevent the occurrence of EMT and revert the cells with the EMT phenotype.[239] Therefore, we further studied whether the rCNPs can result in inhibition of EMT of Hep3B cells.

EMT is important for enhanced tumor progression, invasiveness and metastatic behavior with poor prognosis in clinical patients with liver cancer and several transcription factors such as E-cad, SNAIL and vimentin are engaged in EMT.[240,241] With regard to the EMT, E-cadherin (E-cad) is a tumor suppressor which can prevent tumor metastasis and improve cell-to-cell interactions and adhesive properties. This can prevent cancer cells from metastasizing to distant regions of the body and cause a decrease in EMT.[242–244] In addition, SNAIL is considered an important suppressor of E-cad and plays critical roles in cancer progression. It can promote resistance to drugs, tumor relapse and enhanced metastatic behaviour.[245] Also, vimentin can protect the external stress imposed on cancer cells and help in sustaining organ integrity of tumor tissues during EMT and cancer metastasis.[246] Considering EMT as a therapeutic target can prevent the metastatic behaviour, reduce the invasive properties and inhibit the cancer cells from disseminating to distant sites.[247] The upregulation of E-cad besides the downregulation of SNAIL and vimentin has been reported to reduce the incidence of EMT or reverse the EMT phenotype in cancer cells.[248,249] Therefore, the upregulated expressions of E-cad along with downregulated expressions of SNAIL and vimentin suggest that the rCNPs can prevent the EMT efficiently and mediate cell-killing with the involvement of p53 and NF-κB via ULK1-mediated autophagy (Figure 9).

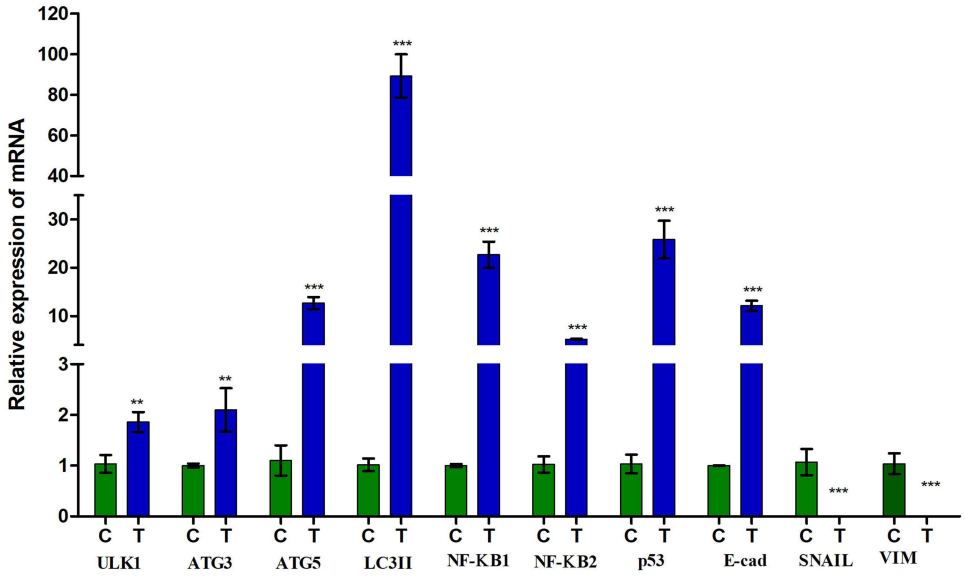

Figure 9 qPCR for analyzing the expression fold of the genes engaged in autophagy and EMT (**p < 0.05, ***p < 0.001).

Cellular Uptake and Internalization of rCNPs

The uptake of nanoparticles less than 200 nm in size predominantly occurs by means of clathrin-mediated and caveolae-mediated endocytosis. This effect is dependent on the mode of contact of the nanoparticles with membrane of the type of cells they interact with, besides the physicochemical characteristics of the nanomaterials such as size, shape and surface charge. As soon as the particle and cells interact at the membrane through adhesion, the membranes undergo elastic deformation and allow diffusion of the polymeric nanomaterials.[250] At the onset of clathrin-mediated endocytosis, it results in the formation of clathrin cages or vesicles in the form of spheres or hexagons due to their surface charge. These vesicles can engulf the nanoparticles in the acidic environment and let them escape the endolysosomal degradation after entry through the plasma membrane. This process is sequential where the nanomaterials are engulfed by the early endosomes, which mature into late endosomes (the pH drops from 6.5 to 5 at this stage in the endolysosomal region) and accumulate into the lysosomes. The cationic polymers with protonated amine groups undergo chelation with protons by proton pumps such as vacuolar-ATPase, causing the pumps to open rigorously. These protons can lead to accumulation of chlorides and water in the lysosomes leading to proton sponge effect (swelling and rupture of lysosomes) and eventually release the cationic nanomaterials (including chitosan) into the cytosol, causing endolysosomal escape.[251]

After they escape the endolysosomal system, they enter the nucleus, cause changes in MMP and result in production and release of excessive ROS leading to mitochondrial DNA degradation and cell death. It is interesting to note that CNPs are specific in targeting cancer cells in comparison to normal cells and positively charged CNPs are taken up at a faster rate by cancer cells in comparison to negatively charged CNPs. This effect might also be attributed to above-said factors such as changes in MMP, ROS and enhanced uptake by cancer cells. Finally, the CNPs are released as debris by exocytosis after their intended functions were achieved.[252]

The pH-responsive release via lysosome-linked pathways can therefore specifically target cancer cells and enter the nucleus besides having no- or limited toxic effects on normal cells.[168] In cancerous cells, the cell death related to lysosomes is primarily integrated with autophagy by the accumulation of autophagosomes. Positively charged nanoparticles usually accumulate in the lysosomes at the initial stages and result in extreme levels of ROS production and cathepsin B besides diffusing into the cytoplasm later by proton sponge effect.[253] Therefore, the increased production of ROS and elevated levels of ULK1, ATG3, ATG5 and critically LC3II observed in our study indicates autophagy has played a key role in the cell death initiated by rCNPs.

The results of our study indicate that after the Hep3B cells were treated with rCNPs-labeled with Rhodamine B and free Rhodamine B, the cellular uptake was higher in cells treated with rCNPs (labeled with Rhodamine B) than the cells treated with free Rhodamine B. With regard to internalization, the nanoparticles were found to predominantly form vesicles within the cytoplasm after 24 hrs and circumvent in the perinuclear space, the cases in which nuclear accumulation was also observed (Figure 10). This means that the rCNPs after being internalized by the cancer cells were effectively taken up by endocytosis and clathrin vesicles were formed at the point of their entry. The observed accumulation of these vesicles in the cytosol may be due to their predominant localization in the lysosomes. The free rCNPs observed in the cytoplasm might be due to endolysosomal escape and lysosomal degradation due to proton sponge effect. After this process, the rCNPs might have entered the nucleus. Hence, the rCNPs follow the processes previously described by the formation of vesicles, endolysosomal escape and accumulation into the nucleus. The rCNPs posed faster cellular uptake and longer retention time up to 24 hrs and were possibly released by exocytosis after drug release. Also, the positive charged rCNPs can also be easily absorbed and can cross the negative charged cancer cell membrane effectively.[254,255]

Biocompatibility of the rCNPs

Safety Evaluation on L929 Fibroblasts

Selective targeting and killing of cancer cells by any drug under trial is usually conducted by analysing the effects on normal fibroblasts such as L929.[256,257] It is generally expected that a tumor-targeting drug is effectively and selectively cytotoxic on cancer cells in comparison to normal cells.[258] The results of the study indicate that the rCNPs were efficient in specific targeting of Hep3B cells in comparison to the normal L929 fibroblasts. This is because the IC_{50} for toxic

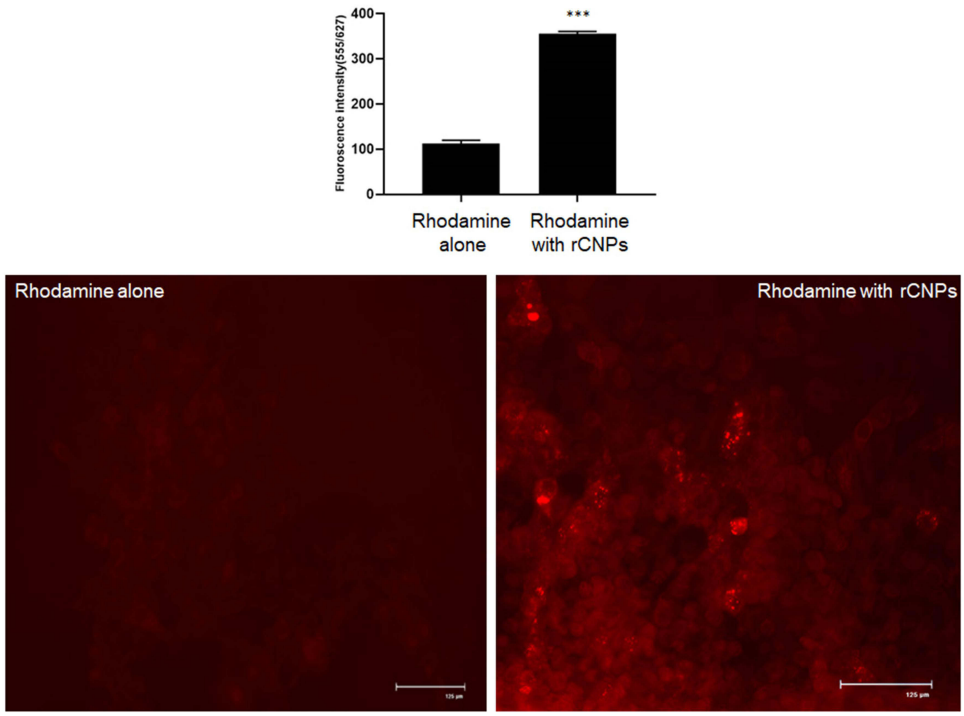

Figure 10 Cellular uptake and internalization of rCNPs into Hep3B cells (*** p >0.001).

effects of rCNPs on the normal fibroblasts was not attained at the maximum-tested dose of 500 µg/mL. Almost 90% of the fibroblasts were viable at this maximum dose tested (Figure 11A). Since the IC_{50} value was not reached at the highest concentration tested, a projected value was predicted following non-linear regression curve fit method using GraphPad Prism which was 2078 ± 0.08 µg/mL. The microscopic observations of the interactions between rCNPs and the fibroblasts are presented in Supplementary Figure 3. As mentioned above, it is widely anticipated that a drug delivering nanoparticulate system should cause enhanced toxic effects on cancer cells and limited toxicity on normal and healthy cells.[259] As expected for nano-drug delivery system, the rCNPs were more toxic on cancerous cells and comparatively exhibited limited toxicity on normal cells.

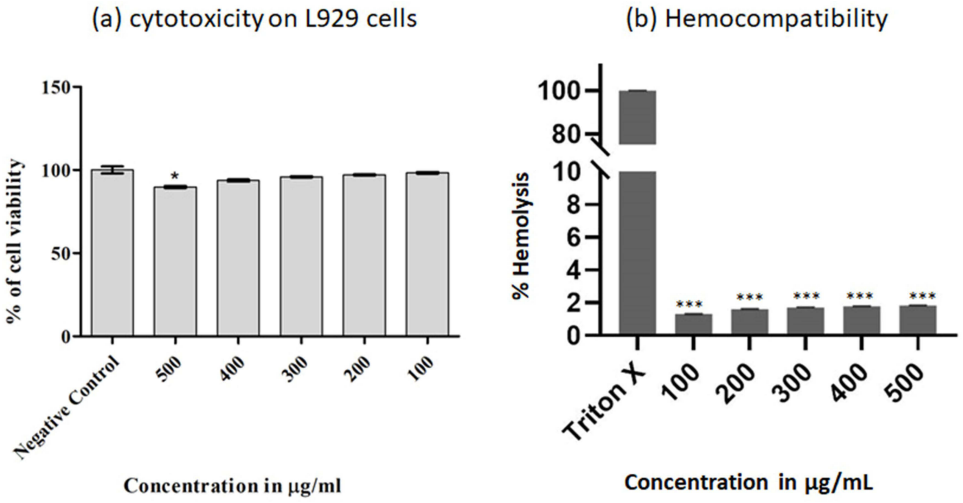

Figure 11 Determination of biocompatibility of rCNPs (**a**) cytotoxic effects on L929 fibroblasts and (**b**) its hemocompatibility. The results were expressed as mean ± SD (*p >0.05, ***p >0.001).

Hemocompatibility of rCNPs

In pursuit of providing a valid assessment of the biocompatibility of a tested material, hemocompatibility is a vital tool. In vitro hemocompatibility testing provides repeatable assays under similar and controllable conditions. This assay therefore validates the use of a material for use in medical applications in vivo. For a drug to be considered potentially effective for use in drug delivery and cancer therapy, it should not cause any unwanted adverse effects on blood. These undesired adverse effects include the formation of thrombus, platelet-leukocyte aggregates, hemolysis and complement activation or other blood-related side effects. To identify the potential suitability of the use of rCNPs in cancer therapy, human blood was used as an in vitro model for testing its compatibility, as in vitro models pose several advantages over direct use of the material in vivo. Enormously controlled in vitro environment for blood flow and anticoagulation has the potential to eliminate factors such as obstructed flow, use of medical interventions and testing without the usage of tissues, making hemolysis assay an attractive option for compatibility testing.[260,261] Although the certain undesired effects of drugs such as elevated bleeding can be minimized by the use of systemic anticoagulants, the use of materials in therapy for longer durations requires the desired use of a material that is significantly hemocompatible.[262] In this process, the physicochemical properties of the preferred nanomaterial determine their hemocompatibility.[263]

The outcomes of the study indicate that the rCNPs are effectively hemocompatible as the maximum-tested concentration of 500 µg/mL induced very low or almost no-hemolytic effects on human blood. The percentage of hemolysis was 1.84% at 500 µg/mL in comparison to the almost 100% (99.56%) lytic effect of 10% Triton X (Figure 11B). In this regard, the percentage of hemolysis at 0–2% is non-hemolytic, whereas 2–5% range exhibit low hemolysis.[264] Since the desired percentage of hemolysis is less than 5%, the rCNPs are safe to use (with non-hemolytic profile) and can be administered intravenously owing to their compatibility with blood.[138]

Conclusions

CNPs were synthesized and loaded with rutin for targeted delivery into Hep3B hepatoblastoma cells. The rCNPs were characterized by standard techniques, and the rutin load was quantitatively measured using UPLC. As the particle size using 5 mg/mL load of rutin seemed ideal, it was used for further studies, and the IC_{50} value for cytotoxic effects on Hep3B cells was 9.7 ± 0.19 µg/mL of rutin. As per our hypothesis, rutin was initially loaded effectively on the rCNPs at 88 µg/mL after being filtered with 0.22 micron filter, and characterization using UV–vis and FTIR further proved the rutin loading. Also, the rCNPs were safe on normal cells as the IC_{50} value was not reached at the maximum-tested concentration of 500 µg/mL on L929 fibroblasts in comparison to the IC_{50} value of 9.7 ± 0.19 µg/mL (rutin load) for Hep3B cells. The rCNPs with particle size of 144.1 nm, PDI of 0.244 and a positive ζ-potential of 16.4 mV were effective in targeted delivery to the sub-cellular organelles after, they undergo escape from lysis by endosomes and lysosomes resulting in proton sponge effect. The in vitro drug release studies indicate that after the escape at endolysosomal pH, the rCNPs may erode or diffuse, resulting in efficient drug release into the nucleus, resulting in genotoxic effects. Owing to their very low hemolytic profile, the rCNPs could be administered intravenously and can release rutin in a sustained manner in the physiological pH (pH 7.4) over longer durations and release rapidly once, they reach the acidic environment of the cancer cells (pH 5.5). As a result, the rCNPs are efficient in pH-responsive targeted delivery of rutin to Hep3B cells.

After the confirmation of rutin loading on rCNPs, determination of physicochemical characteristics and the analysis of their pH-responsive drug release, a steady increase in MMP and ROS was noted in Hep3B cells after treatment with rCNPs. Subsequently, the mechanism for cytotoxic effects of rCNPs on Hep3B cells was found to be related to the activation of NF-κB signaling and ULK1 mediated autophagy besides inhibiting the EMT, thereby preventing metastasis. This is therefore, the first ever international report on determination of the cytotoxic effects and the probable mechanism for such effects of rCNPs on Hep3B cells. Also, the rCNPs possessed excellent hemocompatibility and could be administered intravenously to benefit from pH-responsive drug delivery. In addition, further studies are warranted to identify the potential mechanisms involved in cytotoxic effects of rCNPs on other malignant cells for applications in vivo. This study can therefore significantly improve the usage of CNPs for targeting cancer cells via a drug load, support their candidature for enhanced and targeted drug delivery and manage several malignancies at clinical level effectively in the future.

Acknowledgments

This study was supported by the Changzhou Applied Basic Research Program (CJ20220231), Natural Science Foundation of Jiangsu Province (BK20190138) and Project of Nanjing Municipal Health Commission (ZKX22048).

Disclosure

The authors report no conflicts of interest in this work.

References

1. Thun MJ, DeLancey JO, Center MM, Jemal A, Ward EM. The global burden of cancer: priorities for prevention. *Carcinogenesis*. 2010;31(1):100–110. doi:10.1093/carcin/bgp263
2. Oh JH, Jun DW. The latest global burden of liver cancer: a past and present threat. *Clin Mol Hepatol*. 2023;29(2):355–357. doi:10.3350/cmh.2023.0070
3. Rumgay H, Arnold M, Ferlay J, et al. Global burden of primary liver cancer in 2020 and predictions to 2040. *J Hepatol*. 2022;77(6):1598–1606. doi:10.1016/j.jhep.2022.08.021
4. Siegel RL, Miller KD, Wagle NS, Jemal A. Cancer statistics, 2023. *Ca a Cancer J Clinicians*. 2023;73(1):17–48. doi:10.3322/caac.21763
5. Xia C, Dong X, Li H, et al. Cancer statistics in China and United States, 2022: profiles, trends, and determinants. *Chin Med J*. 2022;135(5):584–590. doi:10.1097/CM9.0000000000002108
6. Raza A, Sood GK. Hepatocellular carcinoma review: current treatment, and evidence-based medicine. *World J Gastroenterol*. 2014;20(15):4115–4127. doi:10.3748/wjg.v20.i15.4115
7. Psilopatis I, Damaskos C, Garmpi A, et al. FDA-approved monoclonal antibodies for unresectable hepatocellular carcinoma: what do we know so far? *Int J Mol Sci*. 2023;24(3):2685. doi:10.3390/ijms24032685
8. Senapati S, Mahanta AK, Kumar S, Maiti P. Controlled drug delivery vehicles for cancer treatment and their performance. *Signal Transduct Target Ther*. 2018;3(1):7. doi:10.1038/s41392-017-0004-3
9. Narvekar M, Xue HY, Eoh JY, Wong HL. Nanocarrier for poorly water-soluble anticancer drugs--barriers of translation and solutions. *AAPS Pharm Sci Tech*. 2014;15(4):822–833. doi:10.1208/s12249-014-0107-x
10. Patra JK, Das G, Fraceto LF, Campos EVR, Rodriguez-Torres MDP. Nano based drug delivery systems: recent developments and future prospects. *J Nanobiotechnol*. 2018;16(1):71. doi:10.1186/s12951-018-0392-8
11. Prasad M, Lambe UP, Brar B, et al. Nanotherapeutics: an insight into healthcare and multi-dimensional applications in medical sector of the modern world. *Biomed. Pharmacother.* 2018;97:1521–1537. doi:10.1016/j.biopha.2017.11.026
12. Yadav P, Bandyopadhyay A, Chakraborty A, Sarkar K. Enhancement of anticancer activity and drug delivery of chitosan-curcumin nanoparticle via molecular docking and simulation analysis. *Carbohydr Polym*. 2018;182:188–198. doi:10.1016/j.carbpol.2017.10.102
13. Witika BA, Makoni PA, Matafwali SK, et al. Biocompatibility of biomaterials for nanoencapsulation: current approaches. *Nanomaterials*. 2020;10(9):1649. doi:10.3390/nano10091649
14. Mohammed MA, Syeda JTM, Wasan KM, Wasan EK. An overview of chitosan nanoparticles and its application in non-parenteral drug delivery. *Pharmaceutics*. 2017;9(4):53. doi:10.3390/pharmaceutics9040053
15. Yanat M, Schroën K. Preparation methods and applications of chitosan nanoparticles; with an outlook toward reinforcement of biodegradable packaging. *React Funct Polym*. 2021;161:104849. doi:10.1016/j.reactfunctpolym.2021.104849
16. Sachdeva B, Sachdeva P, Negi A, et al. Chitosan nanoparticles-based cancer drug delivery: application and challenges. *Mar Drugs*. 2023;21(4):211. doi:10.3390/md21040211
17. Loutfy SA, El-Din HMA, Elberry MH, Allam NG, Hasanin M, Abdellah AM. Synthesis, characterization and cytotoxic evaluation of chitosan nanoparticles: in vitro liver cancer model. *Adv Nat Sci*. 2016;7(3):035008.
18. Quagliariello V, Masarone M, Armenia E, et al. Chitosan-coated liposomes loaded with butyric acid demonstrate anticancer and anti-inflammatory activity in human hepatoma HepG2 cells. *Oncol Rep*. 2019;41(3):1476–1486. doi:10.3892/or.2018.6932
19. Pan Q, Lv Y, Williams GR, et al. Lactobionic acid and carboxymethyl chitosan functionalized graphene oxide nanocomposites as targeted anticancer drug delivery systems. *Carbohydr Polym*. 2016;151:812–820. doi:10.1016/j.carbpol.2016.06.024
20. Qi X, Rui Y, Fan Y, Chen H, Ma N, Wu Z. Galactosylated chitosan-grafted multiwall carbon nanotubes for pH-dependent sustained release and hepatic tumor-targeted delivery of doxorubicin in vivo. *Colloids Surf B*. 2015;133:314–322. doi:10.1016/j.colsurfb.2015.06.003
21. Chavda VP, Balar PC, Patel SB. Interventional nanotheranostics in hepatocellular carcinoma. *Nanotheranostics*. 2023;7(2):128. doi:10.7150/ntno.80120
22. B-l Y, Zheng R, Ruan X-J, Zheng Z-H, Cai H-J. Chitosan-coated doxorubicin nano-particles drug delivery system inhibits cell growth of liver cancer via p53/PRC1 pathway. *Biochem. Biophys. Res. Commun.* 2018;495(1):414–420. doi:10.1016/j.bbrc.2017.10.156
23. Mintz KJ, Leblanc RM. The use of nanotechnology to combat liver cancer: progress and perspectives. *Bioch et Bioph Acta*. 2021;1876(2):188621. doi:10.1016/j.bbcan.2021.188621
24. Bonferoni MC, Gavini E, Rassu G, Maestri M, Giunchedi P. Chitosan Nanoparticles for Therapy and Theranostics of Hepatocellular Carcinoma (HCC) and Liver-Targeting. *Nanomaterials Basel*. 2020;10(5):870. doi:10.3390/nano10050870
25. Guadarrama-Escobar OR, Serrano-Castañeda P, Anguiano-Almazán E, et al. Chitosan nanoparticles as oral drug carriers. *Int J Mol Sci*. 2023;24(5):4289. doi:10.3390/ijms24054289
26. Fathi M, Zangabad PS, Majidi S, Barar J, Erfan-Niya H, Omidi Y. Stimuli-responsive chitosan-based nanocarriers for cancer therapy. *Bioimpacts*. 2017;7(4):269. doi:10.15171/bi.2017.32
27. Ganeshpurkar A, Saluja AK. The pharmacological potential of rutin. *Saudi Pharmac J*. 2017;25(2):149–164. doi:10.1016/j.jsps.2016.04.025
28. Vachirapatama N, Chamna B. Separation and determination of rutin in apples by high performance liquid chromatography. *Sci Technol Asia*. 2012;2012:27–33.

29. Vachirapatama N, Chamnankid B, Kachonpadungkitti Y. Determination of rutin in buckwheat tea and Fagopyrum tataricum seeds by high performance liquid chromatography and capillary electrophoresis. *Journal of Food and Drug Analysis*. 2011;19(4):18.
30. Pandey P, Khan F, Qari HA, Oves M. Rutin (Bioflavonoid) as cell signaling pathway modulator: prospects in treatment and chemoprevention. *Pharmaceuticals*. 2021;14(11):1069. doi:10.3390/ph14111069
31. Qanash H, Al-Rajhi AMH, Almashjary MN, Basabrain AA, Hazzazi MS, Abdelghany TM. Inhibitory potential of rutin and rutin nano-crystals against Helicobacter pylori, colon cancer, hemolysis and Butyrylcholinesterase in vitro and in silico. *Appl Biol Chem*. 2023;66(1):79. doi:10.1186/s13765-023-00832-z
32. Semwal R, Joshi SK, Semwal RB, Semwal DK. Health benefits and limitations of rutin - A natural flavonoid with high nutraceutical value. *Phytochem Lett*. 2021;46:119–128. doi:10.1016/j.phytol.2021.10.006
33. Nouri Z, Fakhri S, Nouri K, Wallace CE, Farzaei MH, Bishayee A. Targeting multiple signaling pathways in cancer: the rutin therapeutic approach. *Cancers*. 2020;12(8):2276. doi:10.3390/cancers12082276
34. Aydin RST, Pulat M. 5-Fluorouracil encapsulated chitosan nanoparticles for pH-stimulated drug delivery: evaluation of controlled release kinetics. *J Nanomater*. 2012;2012:42–42.
35. Naeem A, Yu C, Zang Z, Zhu W, Deng X, Guan Y. Synthesis and evaluation of rutin-hydroxypropyl β-cyclodextrin inclusion complexes embedded in xanthan gum-based (HPMC-g-AMPS) hydrogels for oral controlled drug delivery. *Antioxidants*. 2023;12(3). doi:10.3390/antiox12030552
36. Luo S, Fu Y, Ye J, Liu C. Encapsulation of rutin in protein nanoparticles by pH-driven method: impact of rutin solubility and mechanisms. *J Sci Food Agric*. 2024;104(3):1804–1812. doi:10.1002/jsfa.13068
37. Satari A, Ghasemi S, Habtemariam S, Asgharian S, Lorigooini Z. Rutin: a flavonoid as an effective sensitizer for anticancer therapy; insights into multifaceted mechanisms and applicability for combination therapy. *Evid Based Complement Alternat Med*. 2021;2021. doi:10.1155/2021/9913179
38. Han Y, Wang L, Jiang W, et al. An enhanced stability nanoparticle preparation by corn protein hydrolysate-carboxymethyl chitosan Maillard conjugates loaded with rutin. *Journal of Food Science*. 2019;84(7):1829–1835. doi:10.1111/1750-3841.14616
39. Ahmad N, Ahmad R, Naqvi AA, et al. Quantification of rutin in rat's brain by UHPLC/ESI-Q-TOF-MS/MS after intranasal administration of rutin loaded chitosan nanoparticles. *EXCLI J*. 2016;15:518. doi:10.17179/excli2016-361
40. Ramaswamy S, Dwarampudi LP, Kadiyala M, et al. Formulation and characterization of chitosan encapsulated phytoconstituents of curcumin and rutin nanoparticles. *Int J Biol Macromol*. 2017;104:1807–1812. doi:10.1016/j.ijbiomac.2017.06.112
41. Chang C, Zhang L, Miao Y, Fang B, Yang Z. Anticancer and apoptotic-inducing effects of rutin-chitosan nanoconjugates in triple negative breast cancer cells. *Journal of Cluster Science*. 2021;32(2):331–340. doi:10.1007/s10876-020-01792-w
42. Devi KR, Paulraj SJ, Shah Y, Kumar SR, Kejamurthy P. Chitosan-tripolyphosphate nanoparticles encapsulated rutin targeting bacterial growth inhibition and its cytotoxicity on PANC-1 pancreatic adenocarcinoma cell. *J Appl Pharm Sci*. 2023;13(4):141–148.
43. Ahmad N, Ahmad R, Naqvi AA, et al. Rutin-encapsulated chitosan nanoparticles targeted to the brain in the treatment of Cerebral Ischemia. *Int J Biol Macromol*. 2016;91:640–655. doi:10.1016/j.ijbiomac.2016.06.001
44. Cosco D, Failla P, Costa N, et al. Rutin-loaded chitosan microspheres: characterization and evaluation of the anti-inflammatory activity. *Carbohydr Polym*. 2016;152:583–591. doi:10.1016/j.carbpol.2016.06.039
45. Nandana CN, Christeena M, Bharathi D. Synthesis and characterization of chitosan/silver nanocomposite using rutin for antibacterial, antioxidant and photocatalytic applications. *Journal of Cluster Science*. 2021;33:1–11.
46. Sionkowska A, Lewandowska K, Kurzawa M. Chitosan-based films containing rutin for potential cosmetic applications. *Polymers*. 2023;15(15):3224. doi:10.3390/polym15153224
47. Tran NQ, Joung YK, Lih E, Park KD. In situ forming and rutin-releasing chitosan hydrogels as injectable dressings for dermal wound healing. *Biomacromolecules*. 2011;12(8):2872–2880. doi:10.1021/bm200326g
48. Abhishek Singh T, Sadhukhan P, Ghosh N, et al. Targeted delivery of rutin into breast cancer cells via using phenylboronic acid functionalized MgO nanoparticles. *Materials Science and Engineering: B*. 2023;296:116623. doi:10.1016/j.mseb.2023.116623
49. Li Y, Guo J, Gong X, et al. Inhibitory effects of platinum nanoparticles coated with polyethylene glycol and conjugated with Rutin on the MCF-7 breast cancer cell line. *Arabian J Chem*. 2024;17(3):105567. doi:10.1016/j.arabjc.2023.105567
50. Sathiyaseelan A, Saravanakumar K, Manivasagan P, Jeong MS, Jang E-S, Wang M-H. Folic acid conjugated chitosan encapsulated palladium nanoclusters for NIR triggered photothermal breast cancer treatment. *Carbohydr Polym*. 2022;280:119021. doi:10.1016/j.carbpol.2021.119021
51. Paudel KR, Wadhwa R, Tew XN, et al. Rutin loaded liquid crystalline nanoparticles inhibit non-small cell lung cancer proliferation and migration in vitro. *Life Sci*. 2021;276:119436. doi:10.1016/j.lfs.2021.119436
52. Hoai TT, Yen PT, Dao TTB, et al. Evaluation of the cytotoxic effect of rutin prenanoemulsion in lung and colon cancer cell lines. *J Nanomater*. 2020;2020:1–11. doi:10.1155/2020/8867669
53. Caparica R, Júlio A, Araújo MEM, et al. Anticancer Activity of Rutin and Its Combination with Ionic Liquids on Renal Cells. *Biomolecules*. 2020;10(2):233. doi:10.3390/biom10020233
54. Memar MY, Dalir Abdolahinia E, Yekani M, Kouhsoltani M, Sharifi S, Maleki Dizaj S. Preparation of rutin-loaded mesoporous silica nanoparticles and evaluation of its physicochemical, anticancer, and antibacterial properties. *Mol Bio Rep*. 2023;50(1):203–213. doi:10.1007/s11033-022-07953-6
55. Al-Ekaid NM, Al-Samydai A, Al-deeb I, Nsairat H, Khleifat K, Alshaer W. Preparation, characterization, and anticancer activity of pegylated nano liposomal loaded with rutin against human carcinoma cells (HT-29). *Chem Biodivers*. 2023;20(11):e202301167. doi:10.1002/cbdv.202301167
56. Kunjiappan S, Panneerselvam T, Somasundaram B, et al. Design, in silico modeling, biodistribution study of rutin and quercetin loaded stable human hair keratin nanoparticles intended for anticancer drug delivery. *Biomed Phys Eng Express*. 2018;4(2):025019. doi:10.1088/2057-1976/aaa1cf
57. Pandian SRK, Pavadai P, Vellaisamy S, et al. Formulation and evaluation of rutin-loaded solid lipid nanoparticles for the treatment of brain tumor. *Naunyn-Schmiedeberg's Arch Pharmacol*. 2021;394:735–749. doi:10.1007/s00210-020-02015-9
58. AbouSamra MM, Afifi SM, Galal AF, Kamel R. Rutin-loaded Phyto-Sterosomes as a potential approach for the treatment of hepatocellular carcinoma: in-vitro and in-vivo studies. *J Drug Delivery Sci Technol*. 2023;79:104015. doi:10.1016/j.jddst.2022.104015
59. Pandey P, Rahman M, Bhatt PC, et al. Implication of nano-antioxidant therapy for treatment of hepatocellular carcinoma using PLGA nanoparticles of rutin. *Nanomedicine*. 2018;13(8):849–870. doi:10.2217/nnm-2017-0306

60. Abbasi M, Gholizadeh R, Kasaee SR, et al. An intriguing approach toward antibacterial activity of green synthesized Rutin-templated mesoporous silica nanoparticles decorated with nanosilver. *Sci Rep*. 2023;13(1):5987. doi:10.1038/s41598-023-33095-1
61. Memar MY, Yekani M, Sharifi S, Dizaj SM. Antibacterial and biofilm inhibitory effects of rutin nanocrystals. *Biointerface Res Appl Chem*. 2022;13:132.
62. Abhishek Singh T, Kundu M, Chatterjee S, et al. Synthesis of Rutin loaded nanomagnesia as a smart nanoformulation with significant antibacterial and antioxidant properties. *Inorg Chem Commun*. 2022;140:109492. doi:10.1016/j.inoche.2022.109492
63. Kamel R, Mostafa DM. Rutin nanostructured lipid cosmeceutical preparation with sun protective potential. *J Photochem Photobiol B Biol*. 2015;153:59–66. doi:10.1016/j.jphotobiol.2015.09.002
64. Mohamed KM, Abdelfattah MS, El-khadragy M, et al. Rutin-loaded selenium nanoparticles modulated the redox status, inflammatory, and apoptotic pathways associated with pentylenetetrazole-induced epilepsy in mice. *Green Processing and Synthesis*. 2023;12(1):20230010. doi:10.1515/gps-2023-0010
65. Çetin FK, Ateş SC. In vitro investigation of Rutin-loaded PLGA nanoparticles on leishmania infantum promastigotes. *Süleyman Demirel Üniversitesi Fen Bilimleri Enstitüsü Dergisi*. 2022;26(3):427–434. doi:10.19113/sdufenbed.1074029
66. Surendran V, Palei NN. Formulation and characterization of rutin loaded chitosan-alginate nanoparticles: antidiabetic and cytotoxicity studies. *Current Drug Delivery*. 2022;19(3):379–394. doi:10.2174/1567201818666211005090656
67. Qi L, Xu Z, Jiang X, Hu C, Zou X. Preparation and antibacterial activity of chitosan nanoparticles. *Carbohydr. Res*. 2004;339(16):2693–2700. doi:10.1016/j.carres.2004.09.007
68. Lu E, Franzblau S, Onyuksel H, Popescu C. Preparation of aminoglycoside-loaded chitosan nanoparticles using dextran sulphate as a counterion. *J Microencapsul*. 2009;26(4):346–354. doi:10.1080/02652040802365182
69. Siva D, Abinaya S, Rajesh D, et al. Mollification of doxorubicin (DOX)-mediated cardiotoxicity using conjugated chitosan nanoparticles with supplementation of propionic acid. *Nanomaterials*. 2022;12(3):502. doi:10.3390/nano12030502
70. Al-Kassas R, Wen J, Cheng AE-M, Kim AM-J, Liu SSM, Yu J. Transdermal delivery of propranolol hydrochloride through chitosan nanoparticles dispersed in mucoadhesive gel. *Carbohydr Polym*. 2016;153:176–186. doi:10.1016/j.carbpol.2016.06.096
71. Kouchak M, Azarpanah A. Preparation and in vitro evaluation of chitosan nanoparticles containing diclofenac using the ion-gelation method. *Jundishapur J Nat Pharm Prod*. 2015;10(2):e23082. doi:10.17795/jjnpp-23082
72. Hafizi T, Shahriari MH, Abdouss M, Kahdestani SA. Synthesis and characterization of vancomycin-loaded chitosan nanoparticles for drug delivery. *Polym Bull*. 2023;80(5):5607–5621. doi:10.1007/s00289-022-04237-8
73. Kiaie N, Aghdam RM, Tafti SH, Emami SH. Statistical optimization of chitosan nanoparticles as protein vehicles, using response surface methodology. *J Appl Biomat Funct Mat*. 2016;14(4):413–422. doi:10.5301/jabfm.5000278
74. Simpson E, Sarwar H, Jack I, Lowry D. Evaluation of the potential of chitosan nanoparticles as a delivery vehicle for gentamicin for the treatment of osteomyelitis. *Antibiotics*. 2024;13(3):208. doi:10.3390/antibiotics13030208
75. Bahreini E, Aghaiypour K, Abbasalipourkabir R, Mokarram AR, Goodarzi MT, Saidijam M. Preparation and nanoencapsulation of l-asparaginase II in chitosan-tripolyphosphate nanoparticles and in vitro release study. *Nanoscale Res Lett*. 2014;9(1):340. doi:10.1186/1556-276X-9-340
76. Calvo P, Remunan-Lopez C, Vila-Jato JL, Alonso M. Novel hydrophilic chitosan-polyethylene oxide nanoparticles as protein carriers. *J Appl Polym Sci*. 1997;63(1):125–132. doi:10.1002/(SICI)1097-4628(19970103)63:1<125::AID-APP13>3.0.CO;2-4
77. Sreekumar S, Goycoolea FM, Moerschbacher BM, Rivera-Rodriguez GR. Parameters influencing the size of chitosan-TPP nano- and microparticles. *Sci Rep*. 2018;8(1):4695. doi:10.1038/s41598-018-23064-4
78. Ways TMM, Filippov SK, Maji S, et al. Mucus-penetrating nanoparticles based on chitosan grafted with various non-ionic polymers: synthesis, structural characterisation and diffusion studies. *J Colloid Interface Sci*. 2022;626:251–264. doi:10.1016/j.jcis.2022.06.126
79. Di Martino A, Kucharczyk P, Capakova Z, Humpolicek P, Sedlarik V. Enhancement of temozolomide stability by loading in chitosan-carboxylated polylactide-based nanoparticles. *J Nanopart Res*. 2017;19(2):71. doi:10.1007/s11051-017-3756-3
80. Bozkir A, Saka OM. Chitosan nanoparticles for plasmid DNA delivery: effect of chitosan molecular structure on formulation and release characteristics. *Drug Delivery*. 2004;11(2):107–112. doi:10.1080/10717540490280705
81. Gregoriou Y, Gregoriou G, Yilmaz V, et al. Resveratrol loaded polymeric micelles for theranostic targeting of breast cancer cells. *Nanotheranostics*. 2021;5(1):113–124. doi:10.7150/ntno.51955
82. Wadher K, Trivedi S, Rarokar N, Umekar M. Development and assessment of rutin loaded transfersomes to improve ex vivo membrane permeability and in vitro efficacy. *Hybrid Advances*. 2024;5:100144. doi:10.1016/j.hybadv.2024.100144
83. Alam MS, Sultana N, Rashid MA, et al. Quality by design-optimized glycerosome-enabled nanosunscreen gel of rutin hydrate. *Gels*. 2023;9(9):752. doi:10.3390/gels9090752
84. Opatha SAT, Titapiwatanakun V, Chutoprapat R. Transfersomes: a promising nanoencapsulation technique for transdermal drug delivery. *Pharmaceutics*. 2020;12(9):855. doi:10.3390/pharmaceutics12090855
85. Ramachandran R, Shanmughavel P. Preparation and characterization of biopolymeric nanoparticles used in drug delivery. *Indian J Bioch BIoph*. 2010;47:56–59.
86. Khadke S, Roces CB, Donaghey R, Giacobbo V, Su Y, Perrie Y. Scalable solvent-free production of liposomes. *J Pharm Pharmacol*. 2020;72(10):1328–1340. doi:10.1111/jphp.13329
87. Teng Z, Yu M, Ding Y, et al. Preparation and characterization of nimodipine-loaded nanostructured lipid systems for enhanced solubility and bioavailability. *Int j Nanomed*. 2019;14:119–133. doi:10.2147/IJN.S186899
88. Sultan MH, Moni SS, Madkhali OA, et al. Characterization of cisplatin-loaded chitosan nanoparticles and rituximab-linked surfaces as target-specific injectable nano-formulations for combating cancer. *Sci Rep*. 2022;12(1):468. doi:10.1038/s41598-021-04427-w
89. Singh A, Kar AK, Singh D, et al. pH-responsive eco-friendly chitosan modified cenosphere/alginate composite hydrogel beads as carrier for controlled release of Imidacloprid towards sustainable pest control. *Chem Eng J*. 2022;427:131215. doi:10.1016/j.cej.2021.131215
90. Anitha A, Maya S, Deepa N, et al. Efficient water soluble O-carboxymethyl chitosan nanocarrier for the delivery of curcumin to cancer cells. *Carbohydr Polym*. 2011;83(2):452–461. doi:10.1016/j.carbpol.2010.08.008
91. Florento L, Matias R, Tuaño E, Santiago K, Dela Cruz F, Tuazon A. Comparison of cytotoxic activity of anticancer drugs against various human tumor cell lines using in vitro cell-based approach. *Int j Biomed Sci*. 2012;8(1):76. doi:10.59566/IJBS.2012.8076

92. Biswas R, Mondal A, Chatterjee S, Ahn J. Evaluation of synergistic effects of sulforaphene with photodynamic therapy in human cervical cancer cell line. *Lasers Med Sci*. 2016;31(8):1675–1682. doi:10.1007/s10103-016-2037-1
93. Jakic B, Buszko M, Cappellano G, Wick G. Elevated sodium leads to the increased expression of HSP60 and induces apoptosis in HUVECs. *PLoS One*. 2017;12(6):e0179383. doi:10.1371/journal.pone.0179383
94. Ling L, Tan K, Lin H, Chiu G. The role of reactive oxygen species and autophagy in safingol-induced cell death. *Cell Death Dis*. 2011;2(3): e129–e129. doi:10.1038/cddis.2011.12
95. Livak KJ, Schmittgen TD. Analysis of relative gene expression data using real-time quantitative PCR and the 2− ΔΔCT method. *methods*. 2001;25(4):402–408. doi:10.1006/meth.2001.1262
96. Hou Z, Zhan C, Jiang Q, et al. Both FA-and mPEG-conjugated chitosan nanoparticles for targeted cellular uptake and enhanced tumor tissue distribution. *Nanoscale Res Lett*. 2011;6:1–11. doi:10.1186/1556-276X-6-563
97. Seisel Q, Pelletier F, Deshayes S, Boisguerin P. How to evaluate the cellular uptake of CPPs with fluorescence techniques: dissecting methodological pitfalls associated to tryptophan-rich peptides. *Bioch et Bioph Acta*. 2019;1861(9):1533–1545. doi:10.1016/j.bbamem.2019.06.011
98. Shahjahan A, Sekar S, Kasinathan K, ArulJothi KN. The cytotoxic and anti-tumor potential of methanolic extracts of Indian marine isolates in HCT116 colorectal cancer cells. *Anti Can Agent Med Chem*. 2023;23(17):1974–1981.
99. Cocean G, Cocean A, Postolachi C, Garofalide S, Bulai G. High-power laser deposition of chitosan polymers: medical and environmental applications. *Polymers*. 2022;14(8):1537. doi:10.3390/polym14081537
100. El-Naggar NE-A, Shiha AM, Mahrous H, Mohammed ABA. Green synthesis of chitosan nanoparticles, optimization, characterization and antibacterial efficacy against multi drug resistant biofilm-forming Acinetobacter baumannii. *Sci Rep*. 2022;12(1):19869. doi:10.1038/s41598-022-24303-5
101. Yahya R, Al-Rajhi AMH, Alzaid SZ, et al. Molecular docking and efficacy of aloe vera gel based on chitosan nanoparticles against helicobacter pylori and its antioxidant and anti-inflammatory activities. *Polymers*. 2022;14(15):2994. doi:10.3390/polym14152994
102. Duraisamy N, Dhayalan S, Shaik MR, Shaik AH, Shaik JP, Shaik B. Green synthesis of chitosan nanoparticles using of martynia annua l. ethanol leaf extract and their antibacterial activity. *Crystals*. 2022;12(11):1550. doi:10.3390/cryst12111550
103. Abualhasan MN, Mansour J, Jaradat N, Zaid AN, Khadra I. Formulation and development of a validated UV-spectrophotometric analytical method of rutin tablet. *Int Scholarly Res Notices*. 2017;2017:1–7. doi:10.1155/2017/2624947
104. Ganesan S, Alagarasan JK, Sonaimuthu M, et al. Preparation and characterization of salsalate-loaded chitosan nanoparticles: in vitro release and antibacterial and antibiofilm activity. *Mar Drugs*. 2022;20(12):733. doi:10.3390/md20120733
105. Chen D, Liu Y, Liu P, Zhou Y, Jiang L. Orally delivered rutin in lipid-based nano-formulation exerts strong antithrombotic effects by protein disulfide isomerase inhibition. *Drug Delivery*. 2022;29(1):1824–1835. doi:10.1080/10717544.2022.2083726
106. Kızılbey K. Optimization of rutin-loaded PLGA nanoparticles synthesized by single-emulsion solvent evaporation method. *Acs Omega*. 2019;4 (1):555–562. doi:10.1021/acsomega.8b02767
107. Ciro Y, Rojas J, Di Virgilio AL, Alhajj MJ, Carabali GA, Salamanca CH. Production, physicochemical characterization, and anticancer activity of methotrexate-loaded phytic acid-chitosan nanoparticles on HT-29 human colon adenocarcinoma cells. *Carbohydr Polym*. 2020;243:116436. doi:10.1016/j.carbpol.2020.116436
108. Choudhary RC, Kumari S, Kumaraswamy R, et al. Characterization methods for chitosan-based nanomaterials. *Plant Nanobionics*. 2019;1:103–116.
109. Lustriane C, Dwivany FM, Suendo V, Reza M. Effect of chitosan and chitosan-nanoparticles on post harvest quality of banana fruits. *J Plant Biotechnol*. 2018;45(1):36–44. doi:10.5010/JPB.2018.45.1.036
110. Thai H, Thuy Nguyen C, Thi Thach L, et al. Characterization of chitosan/alginate/lovastatin nanoparticles and investigation of their toxic effects in vitro and in vivo. *Sci Rep*. 2020;10(1):1–15. doi:10.1038/s41598-020-57666-8
111. Goodarzi A, Khanmohammadi M, Ebrahimi-Barough S, et al. Alginate-based hydrogel containing taurine-loaded chitosan nanoparticles in biomedical application. *Arch Neurosci*. 2019;6(2):1.
112. Kain D, Kumar S. Synthesis and characterization of chitosan nanoparticles of Achillea millefolium L. and their activities. *F1000Research*. 2020;9:1297. doi:10.12688/f1000research.26446.1
113. Mahmood MA, Madni A. Ionically cross-linked chitosan nanoparticles for sustained delivery of docetaxel: fabrication. *Post-Formul Acute Oral Toxicity Eval*. 2019;14:10035–10046.
114. El-Houssiny A, Ward A, Mostafa D, et al. Drug–polymer interaction between glucosamine sulfate and alginate nanoparticles: FTIR, DSC and dielectric spectroscopy studies. *Adv Nat Sci*. 2016;7(2):025014.
115. Ahmad N, Khan MR, Palanisamy S, Mohandoss S. Anticancer drug-loaded chitosan nanoparticles for in vitro release, promoting antibacterial and anticancer activities. *Polymers*. 2023;15(19):3925. doi:10.3390/polym15193925
116. IAd L, Khalil NM, Mainardes RM. A stability-indicating HPLC-PDA method for the determination of ferulic acid in chitosan-coated poly (lactide-co-glycolide) nanoparticles. *Braz J Pharm Sci*. 2017;2017:53.
117. Pramod K, Ilyas UK, Kamal YT, Ahmad S, Ansari SH, Ali J. Development and validation of RP-HPLC-PDA method for the quantification of eugenol in developed nanoemulsion gel and nanoparticles. *J Anal Sci Technol*. 2013;4(1):16. doi:10.1186/2093-3371-4-16
118. Güven UM, Berkman MS, Yazan Y. Development and validation of UPLC method for the determination of olopatadine hydrochloride in polymeric nanoparticles. *Acta Pharm Sci*. 2019;57:7–18.
119. Danaei M, Dehghankhold M, Ataei S, et al. Impact of particle size and polydispersity index on the clinical applications of lipidic nanocarrier systems. *Pharmaceutics*. 2018;10(2):57. doi:10.3390/pharmaceutics10020057
120. Li C, Chen L, McClements DJ, et al. Preparation and characterization of rutin–loaded zein–carboxymethyl starch nanoparticles. *Foods*. 2022;11 (18):2827. doi:10.3390/foods11182827
121. Saha S, Mishra A. A facile preparation of rutin nanoparticles and its effects on controlled growth and morphology of calcium oxalate crystals. *Journal of Crystal Growth*. 2020;540:125635. doi:10.1016/j.jcrysgro.2020.125635
122. AbdElrazek DA, Hassan NH, Ibrahim MA, Hassanen EI, Farroh KY, Abass HI. Ameliorative effects of rutin and rutin-loaded chitosan nanoparticles on testicular oxidative stress and histological damage induced by cyclophosphamide in male rats. *Food and Chemical Toxicology*. 2024;184:114436. doi:10.1016/j.fct.2024.114436

123. Sri KV, Santhoshini G, Sankar DR, Niharika K. Formulation and evaluation of rutin loaded nanosponges. *Asian J Res Pharmac Sci*. 2018;8(1):21–24. doi:10.5958/2231-5659.2018.00005.X
124. Ardani H, Imawan C, Handayani W, Djuhana D, Harmoko A, Fauzia V Enhancement of the stability of silver nanoparticles synthesized using aqueous extract of Diospyros discolor Willd. leaves using polyvinyl alcohol. Paper presented at: IOP Conference Series: Materials Science and Engineering; 2017.
125. Maguire CM, Rösslein M, Wick P, Prina-Mello A. Characterisation of particles in solution–a perspective on light scattering and comparative technologies. *Sci Technol Adv Mater*. 2018;19(1):732–745. doi:10.1080/14686996.2018.1517587
126. Erdogan O, Abbak M, Demirbolat GM, et al. Green synthesis of silver nanoparticles via Cynara scolymus leaf extracts: the characterization, anticancer potential with photodynamic therapy in MCF7 cells. *PLoS One*. 2019;14(6):e0216496. doi:10.1371/journal.pone.0216496
127. Wen X, Wang Q, Dai T, et al. Identification of possible reductants in the aqueous leaf extract of mangrove plant Rhizophora apiculata for the fabrication and cytotoxicity of silver nanoparticles against human osteosarcoma MG-63 cells. *Mater Sci Eng C*. 2020;116:111252. doi:10.1016/j.msec.2020.111252
128. Sangwan S, Seth R. Nanotechnology: a boon in cancer therapy. *Internat J Nanomat*. 2021;7(1):001–006.
129. Lo Presti E, Pizzolato G, Corsale AM, et al. γδ T Cells and Tumor Microenvironment: from Immunosurveillance to Tumor Evasion. *Front Immunol*. 2018;9:1395–1395. doi:10.3389/fimmu.2018.01395
130. Deshpande PP, Biswas S, Torchilin VP. Current trends in the use of liposomes for tumor targeting. *Nanomedicine (Lond)*. 2013;8(9):1509–1528. doi:10.2217/nnm.13.118
131. Jose Chirayil C, Abraham J, Kumar Mishra R, George SC, Thomas S. Chapter 1 - Instrumental Techniques for the Characterization of Nanoparticles. In: Thomas S, Thomas R, Zachariah AK, Mishra RK, editors. *Thermal and Rheological Measurement Techniques for Nanomaterials Characterization*. Elsevier; 2017:1–36.
132. Clogston JD, Patri AK. Zeta potential measurement. *Meth Mol Bio*. 2011;697:63–70.
133. Lu Y, Qi J, Wu W. Chapter 20 - Lipid nanoparticles: in vitro and in vivo approaches in drug delivery and targeting. In: Grumezescu AM, editor. *Drug Targeting and Stimuli Sensitive Drug Delivery Systems*. William Andrew Publishing; 2018:749–783.
134. Aibani N, Rai R, Patel P. Chitosan nanoparticles at the biological interface: implications for drug delivery. *Antioxidants*. 2021;13(10):1.
135. Piras AM, Maisetta G, Sandreschi S, et al. Chitosan nanoparticles loaded with the antimicrobial peptide temporin B exert a long-term antibacterial activity in vitro against clinical isolates of Staphylococcus epidermidis. *Front Microbiol*. 2015;6:372. doi:10.3389/fmicb.2015.00372
136. Soltanzadeh M, Peighambardoust SH, Ghanbarzadeh B, Mohammadi M, Lorenzo JM. Chitosan nanoparticles as a promising nanomaterial for encapsulation of pomegranate (Punica granatum L.) peel extract as a natural source of antioxidants. *Nanomaterials*. 2021;11(6):1439. doi:10.3390/nano11061439
137. Vogel R, Pal AK, Jambhrunkar S, et al. High-resolution single particle zeta potential characterisation of biological nanoparticles using tunable resistive pulse sensing. *Sci Rep*. 2017;7(1):17479. doi:10.1038/s41598-017-14981-x
138. Zhang L, Hu Y. Alphastatin-loaded chitosan nanoparticle preparation and its antiangiogenic effect on lung carcinoma. *Int J Polym Sci*. 2019;2019:1–9. doi:10.1155/2019/2751384
139. Chigumira W, Maposa P, Gadaga LL, Dube A, Tagwireyi D, Maponga CC. Preparation and evaluation of pralidoxime-loaded PLGA nanoparticles as potential carriers of the drug across the blood brain barrier. *J Nanomater*. 2015;2015:8–8. doi:10.1155/2015/692672
140. Liu X, Shan K, Shao X, et al. Nanotoxic effects of silver nanoparticles on normal HEK-293 cells in comparison to cancerous hela cell line. *Int j Nanomed*. 2021;16:753. doi:10.2147/IJN.S289008
141. Kaasalainen M, Aseyev V, von Haartman E, et al. Size, stability, and porosity of mesoporous nanoparticles characterized with light scattering. *Nanoscale Res Lett*. 2017;12(1):74. doi:10.1186/s11671-017-1853-y
142. Yang G, Liu Y, Wang H, et al. Bioinspired core–shell nanoparticles for hydrophobic drug delivery. *Angew. Chem. Int. Ed.* 2019;58(40):14357–14364. doi:10.1002/anie.201908357
143. De Gaetano F, Cristiano MC, Venuti V, et al. Rutin-loaded solid lipid nanoparticles: characterization and in vitro evaluation. *Molecules*. 2021;26(4):1039. doi:10.3390/molecules26041039
144. Agrahari V, Youan -B-BC. Sensitive and rapid HPLC quantification of tenofovir from hyaluronic acid-based nanomedicine. *AAPS Pharm Sci Tech*. 2012;13:202–210. doi:10.1208/s12249-011-9735-6
145. Vigata M, Meinert C, Hutmacher DW, Bock N. Hydrogels as drug delivery systems: a review of current characterization and evaluation techniques. *Pharmaceutics*. 2020;12(12):1188. doi:10.3390/pharmaceutics12121188
146. Herrera M, Cantos J, Muñoz K, Durán J, Vinueza J, Dos Santos FK. Validation of analytical method by UV spectrophotometric quantification of gemfibrozil incorporated in the microemulsions. *infoANALÍTICA*. 2021;9(1):137–150. doi:10.26807/ia.v9i1.195
147. Libánská A, Špringer T, Peštová L, et al. Using surface plasmon resonance, capillary electrophoresis and diffusion-ordered NMR spectroscopy to study drug release kinetics. *Commun. Chem.* 2023;6(1):180. doi:10.1038/s42004-023-00992-5
148. Dhole SM, Amnerkar ND, Khedekar PB. Comparison of UV spectrophotometry and high performance liquid chromatography methods for the determination of repaglinide in tablets. *Pharm Methods*. 2012;3(2):68–72. doi:10.4103/2229-4708.103875
149. Wang Q, Wang G, Xie S, Zhao X, Zhang Y. Comparison of high-performance liquid chromatography and ultraviolet-visible spectrophotometry to determine the best method to assess Levofloxacin released from mesoporous silica microspheres/nano-hydroxyapatite composite scaffolds. *Exp Ther Med*. 2019;17(4):2694–2702. doi:10.3892/etm.2019.7238
150. Dahiya P, Zafar A, Ahmad FJ, Khalid M, Ali A. Development of Forskolin and rutin-loaded polymeric nanoparticles for enhancement of topical ocular delivery: optimization, in-vitro, ex-vivo, and toxicity evaluation. *J Drug Delivery Sci Technol*. 2023;82:104292. doi:10.1016/j.jddst.2023.104292
151. Yoshida T, Lai TC, Kwon GS, Sako K. pH- and ion-sensitive polymers for drug delivery. *Expert Opin Drug Delivery*. 2013;10(11):1497–1513. doi:10.1517/17425247.2013.821978
152. Lee Y, Thompson DH. Stimuli-responsive liposomes for drug delivery. *Wiley Interdiscip Rev Nanomed Nanobiotechnol*. 2017;9(5). doi:10.1002/wnan.1450
153. AlSawaftah NM, Awad NS, Pitt WG, Husseini GA. pH-responsive nanocarriers in cancer therapy. *Polymers*. 2022;14(5):936. doi:10.3390/polym14050936

154. Yue H, Gou L, Tang Z, Liu Y, Liu S, Tang H. Construction of pH-responsive nanocarriers in combination with ferroptosis and chemotherapy for treatment of hepatocellular carcinoma. *Cancer Nanotechnol*. 2022;13(1):4. doi:10.1186/s12645-022-00111-4
155. Dhawa T, Hazra A, Barma A, Pal K, Karmakar P, Roy P. 4-Methyl-2, 6-diformylphenol based biocompatible chemosensors for pH: discrimination between normal cells and cancer cells. *RSC Adv*. 2020;10(26):15501–15513. doi:10.1039/D0RA00754D
156. Sonju JJ, Dahal A, Singh SS, et al. A pH-sensitive liposome formulation of a peptidomimetic-Dox conjugate for targeting HER2 + cancer. *Int J Pharm*. 2022;612:121364. doi:10.1016/j.ijpharm.2021.121364
157. Saadat M, Mostafaei F, Mahdinloo S, et al. Drug delivery of pH-Sensitive nanoparticles into the liver cancer cells. *J Drug Delivery Sci Technol*. 2021;63:102557. doi:10.1016/j.jddst.2021.102557
158. Ghosh R, Mondal S, Mukherjee D, et al. Oral drug delivery using a polymeric nanocarrier: chitosan nanoparticles in the delivery of rifampicin. *Mater Adv*. 2022;3(11):4622–4628. doi:10.1039/D2MA00295G
159. More KN, Mun S-K, Kang J, Kim -J-J, Yee S-T, Chang D-J. Molecular design of fluorescent pH sensors based on reduced rhodol by structure-pKa relationship for imaging of lysosome. *Dyes Pigm*. 2021;184:108785. doi:10.1016/j.dyepig.2020.108785
160. Wang Q, Zhou L, Qiu L, Lu D, Wu Y, Zhang X-B. An efficient ratiometric fluorescent probe for tracking dynamic changes in lysosomal pH. *Analyst*. 2015;140(16):5563–5569. doi:10.1039/C5AN00683J
161. Zheng Q, Cheng W, Zhang X, Shao R, Li Z. A pH-induced reversible assembly system with resveratrol-controllable loading and release for enhanced tumor-targeting chemotherapy. *Nanoscale Res Lett*. 2019;14(1):305. doi:10.1186/s11671-019-3139-z
162. Gaohua L, Miao X, Dou L. Crosstalk of physiological pH and chemical pKa under the umbrella of physiologically based pharmacokinetic modeling of drug absorption, distribution, metabolism, excretion, and toxicity. *Expert Opin Drug Metab Toxicol*. 2021;17(9):1103–1124. doi:10.1080/17425255.2021.1951223
163. Nasr M, Kira AY, Saber S, Essa EA, El-Gizawy SA. Telmisartan-Loaded lactosylated chitosan nanoparticles as a liver specific delivery system: synthesis, optimization and targeting efficiency. *AAPS Pharm Sci Tech*. 2023;24(6):144. doi:10.1208/s12249-023-02605-9
164. Li L, Zhang X, Pi C, et al. Review of Curcumin Physicochemical Targeting Delivery System. *Int J Nanomed*. 2020;15:9799–9821. doi:10.2147/IJN.S276201
165. Yang Y, Wang Z, Peng Y, Ding J, Zhou W. A Smart pH-sensitive delivery system for enhanced anticancer efficacy via paclitaxel endosomal escape. *Front Pharmacol*. 2019;10:10. doi:10.3389/fphar.2019.00010
166. Herdiana Y, Wathoni N, Shamsuddin S, Muchtaridi M. Drug release study of the chitosan-based nanoparticles. *Heliyon*. 2022;8(1):e08674. doi:10.1016/j.heliyon.2021.e08674
167. Medina-Moreno A, El-Hammadi MM, Arias JL. pH-dependent, extended release and enhanced in vitro efficiency against colon cancer of Tegafur formulated using chitosan-coated poly(ε-caprolactone) nanoparticles. *J Drug Delivery Sci Technol*. 2023;86:104594. doi:10.1016/j.jddst.2023.104594
168. Tian X, Shi A, Yin H, et al. Nanomaterials respond to lysosomal function for tumor treatment. *Cells*. 2022;11(21):3348. doi:10.3390/cells11213348
169. Augustine R, Hasan A, Primavera R, Wilson RJ, Thakor AS, Kevadiya BD. Cellular uptake and retention of nanoparticles: insights on particle properties and interaction with cellular components. *Mater Today Commun*. 2020;25:101692.
170. Dharmayanti C, Gillam TA, Klingler-Hoffmann M, Albrecht H, Blencowe A. Strategies for the development of pH-responsive synthetic polypeptides and polymer-peptide hybrids: recent advancements. *Polymers*. 2021;13(4):624. doi:10.3390/polym13040624
171. Guo K, Liu Y, Ding M, Sun Q, Shubhra QTH. Enhanced drug release from a pH-responsive nanocarrier can augment colon cancer treatment by blocking PD-L1 checkpoint and consuming tumor glucose. *Mater Des*. 2022;219:110824. doi:10.1016/j.matdes.2022.110824
172. Chu S, Shi X, Tian Y, Gao F. pH-responsive polymer nanomaterials for tumor therapy. *Front Oncol*. 2022;12:855019. doi:10.3389/fonc.2022.855019
173. Nallamuthu I, Devi A, Khanum F. Chlorogenic acid loaded chitosan nanoparticles with sustained release property, retained antioxidant activity and enhanced bioavailability. *Asian J Pharm Sci*. 2015;10(3):203–211. doi:10.1016/j.ajps.2014.09.005
174. Shahid N, Erum A, Zaman M, et al. Synthesis and evaluation of chitosan based controlled release nanoparticles for the delivery of ticagrelor. *Des. Monomers Polym*. 2022;25(1):55–63. doi:10.1080/15685551.2022.2054117
175. Imtiyaz Z, He J, Leng Q, Agrawal AK, Mixson AJ. pH-sensitive targeting of tumors with chemotherapy-laden nanoparticles: progress and challenges. *Pharmaceutics*. 2022;14(11):2427. doi:10.3390/pharmaceutics14112427
176. Argitekin E, Ersoz-Gulseven E, Cakan-Akdogan G, Akdogan Y. Dopamine-conjugated bovine serum albumin nanoparticles containing pH-responsive catechol-V (III) coordination for in vitro and in vivo drug delivery. *Biomacromolecules*. 2023;24(8):3603–3618. doi:10.1021/acs.biomac.3c00363
177. Virmani T, Kumar G, Sharma A, et al. Amelioration of cancer employing chitosan, its derivatives, and chitosan-based nanoparticles: recent updates. *Polymers*. 2023;15(13):2928. doi:10.3390/polym15132928
178. Meng F, Cheng R, Deng C, Zhong Z. Intracellular drug release nanosystems. *Mater Today*. 2012;15(10):436–442. doi:10.1016/S1369-7021(12)70195-5
179. Niu N, Wang L. In vitro human cell line models to predict clinical response to anticancer drugs. *Pharmacogenomics*. 2015;16(3):273–285. doi:10.2217/pgs.14.170
180. Pan E, Bogumil D, Cortessis V, Yu S, Nieva J. A systematic review of the efficacy of preclinical models of lung cancer drugs. *Front Oncol*. 2020;10:591. doi:10.3389/fonc.2020.00591
181. Kumar N, Afjei R, Massoud TF, Paulmurugan R. Comparison of cell-based assays to quantify treatment effects of anticancer drugs identifies a new application for Bodipy-L-cystine to measure apoptosis. *Sci Rep*. 2018;8(1):16363. doi:10.1038/s41598-018-34696-x
182. Wadhawan A, Singh J, Sharma H, et al. Anticancer biosurfactant-loaded PLA–PEG nanoparticles induce apoptosis in human MDA-MB-231 breast cancer cells. *ACS omega*. 2022;7(6):5231–5241. doi:10.1021/acsomega.1c06338
183. Yao Y, Zhou Y, Liu L, et al. Nanoparticle-based drug delivery in cancer therapy and its role in overcoming drug resistance. *Front Mol Biosci*. 2020;7:193. doi:10.3389/fmolb.2020.00193
184. Gallego NE, Wray S, Preza E, Abramov AY. Higher mitochondrial membrane potential induces ROS production in the familiar form of frontotemporal dementia with MAPT mutations. *Biophys. J*. 2015;108(2):1.

185. Rovini A, Heslop K, Hunt EG, et al. Quantitative analysis of mitochondrial membrane potential heterogeneity in unsynchronized and synchronized cancer cells. *FASEB J*. 2021;35(1):e21148. doi:10.1096/fj.202001693R
186. Zorova LD, Popkov VA, Plotnikov EY, et al. Mitochondrial membrane potential. *Anal Biochem*. 2018;552:50–59. doi:10.1016/j.ab.2017.07.009
187. Backes S, Herrmann JM. Protein translocation into the intermembrane space and matrix of mitochondria: mechanisms and driving forces. *Front Mol Biosci*. 2017;4:83. doi:10.3389/fmolb.2017.00083
188. Kalvelytė AV, Imbrasaitė A, Krestnikova N, Stulpinas A. Chapter Four - Adult Stem Cells and Anticancer Therapy. In: Fishbein JC, Heilman JM, editors. *Advances in Molecular Toxicology*. Vol. 11. Elsevier; 2017:123–202.
189. Wang Y, Xu E, Musich PR, Lin F. Mitochondrial dysfunction in neurodegenerative diseases and the potential countermeasure. *CNS Neurosci Ther*. 2019;25(7):816–824. doi:10.1111/cns.13116
190. van der Stel W, Yang H, le Dévédec SE, van de Water B, Beltman JB, Danen EHJ. High-content high-throughput imaging reveals distinct connections between mitochondrial morphology and functionality for OXPHOS complex I, III, and V inhibitors. *Cell Biol Toxicol*. 2022;2022:1.
191. Norat P, Soldozy S, Sokolowski JD, et al. Mitochondrial dysfunction in neurological disorders: exploring mitochondrial transplantation. *Npj Regenerat Med*. 2020;5(1):22. doi:10.1038/s41536-020-00107-x
192. Bhatti JS, Bhatti GK, Reddy PH. Mitochondrial dysfunction and oxidative stress in metabolic disorders — a step towards mitochondria based therapeutic strategies. *Bioch et Bioph Acta*. 2017;1863(5):1066–1077. doi:10.1016/j.bbadis.2016.11.010
193. Bagkos G, Koufopoulos K, Piperi C. A new model for mitochondrial membrane potential production and storage. *Med Hypotheses*. 2014;83 (2):175–181. doi:10.1016/j.mehy.2014.05.001
194. Kim SY. Cancer energy metabolism: shutting power off cancer factory. *Biomol Ther*. 2018;26(1):39–44. doi:10.4062/biomolther.2017.184
195. Vultaggio-Poma V, Sarti AC, Di Virgilio F. Extracellular ATP: a Feasible Target for Cancer Therapy. *Cells*. 2020;9(11):2496. doi:10.3390/cells9112496
196. Yang Y, Bai J, Du W, Kong D. The mechanisms of action of mitochondrial targeting agents in cancer: inhibiting oxidative phosphorylation and inducing apoptosis. *Front Pharmacol*. 2023;14:1243613. doi:10.3389/fphar.2023.1243613
197. Lyamzaev KG, Tokarchuk AV, Panteleeva AA, Mulkidjanian AY, Skulachev VP, Chernyak BV. Induction of autophagy by depolarization of mitochondria. *Autophagy*. 2018;14(5):921–924. doi:10.1080/15548627.2018.1436937
198. Johnson TA, Jinnah H, Kamatani N. Shortage of cellular ATP as a cause of diseases and strategies to enhance ATP. *Front Pharmacol*. 2019;10:98. doi:10.3389/fphar.2019.00098
199. Mori K, Uchida T, Yoshie T, et al. A mitochondrial ROS pathway controls matrix metalloproteinase 9 levels and invasive properties in RAS-activated cancer cells. *FEBS J*. 2019;286(3):459–478. doi:10.1111/febs.14671
200. Guo C, Sun L, Chen X, Zhang D. Oxidative stress, mitochondrial damage and neurodegenerative diseases. *Neural Regen Res*. 2013;8 (21):2003–2014. doi:10.3969/j.issn.1673-5374.2013.21.009
201. Manke A, Wang L, Rojanasakul Y. Mechanisms of nanoparticle-induced oxidative stress and toxicity. *Biomed Res Int*. 2013;2013:942916. doi:10.1155/2013/942916
202. Fu PP, Xia Q, Hwang H-M, Ray PC, Yu H. Mechanisms of nanotoxicity: generation of reactive oxygen species. *Journal of Food and Drug Analysis*. 2014;22(1):64–75. doi:10.1016/j.jfda.2014.01.005
203. Aggarwal V, Tuli HS, Varol A, Thakral F, Yerer MB. Role of reactive oxygen species in cancer progression: molecular mechanisms and recent advancements. *Biomolecules*. 2019;9(11):735. doi:10.3390/biom9110735
204. Redza-Dutordoir M, Averill-Bates DA. Activation of apoptosis signalling pathways by reactive oxygen species. *Bioch et Bioph Acta*. 2016;1863 (12):2977–2992. doi:10.1016/j.bbamcr.2016.09.012
205. Perillo B, Di Donato M, Pezone A, et al. ROS in cancer therapy: the bright side of the moon. *Exp. Mol. Med.* 2020;52(2):192–203. doi:10.1038/s12276-020-0384-2
206. Hasan A, Rizvi SF, Parveen S, Pathak N, Nazir A, Mir SS. Crosstalk between ROS and autophagy in tumorigenesis: understanding the multifaceted paradox. *Front Oncol*. 2022;2022:12.
207. Kma L, Baruah TJ. The interplay of ROS and the PI3K/Akt pathway in autophagy regulation. *Feb*. 2022;69(1):248–264.
208. Hoy MA. Chapter 8 - DNA Amplification by the Polymerase Chain Reaction: molecular Biology Made Accessible. In: Hoy MA, editor. *Insect Molecular Genetics*. San Diego: Academic Press; 2013:307–372.
209. Lobert S, Hiser L, Correia JJ. Chapter 4 - Expression Profiling of Tubulin Isotypes and Microtubule-Interacting Proteins Using Real-Time Polymerase Chain Reaction. In: Wilson L, Correia JJ, editors. *Methods in Cell Biology*. Vol 95: Academic Press; 2010:47–58.
210. Ozturk M, Ozsoylemez OD, Dagistanli FK. The detection techniques for autophagy-associated cell death-related genes and proteins: gene expression assay and Immunohistochemistry. *Meth Mol Bio*. 2019;1854:119–130.
211. Jiang Z, Liu J, Chen B, et al. Cytotoxic effects of a sesquiterpene β-elemene on THP-1 leukemia cells is mediated via crosstalk between beclin-1 mediated autophagy and caspase-dependent apoptosis. *Process Biochem*. 2019;87:174–178. doi:10.1016/j.procbio.2019.09.006
212. Amatori S, Persico G, Fanelli M. Real-time quantitative PCR array to study drug-induced changes of gene expression in tumor cell lines. *J Cancer Metastasis Treat*. 2017;3(5):90–99. doi:10.20517/2394-4722.2017.22
213. Levine B, Kroemer G. SnapShot: macroautophagy. *Cell*. 2008;132(1):162.e161–162.e163. doi:10.1016/j.cell.2007.12.026
214. Dong L, He J, Luo L, Wang K. Targeting the interplay of autophagy and ros for cancer therapy: an updated overview on phytochemicals. *Pharmaceuticals*. 2023;16(1). doi:10.3390/ph16010092
215. Trelford CB, Di Guglielmo GM. Canonical and non-canonical TGFβ signaling activate autophagy in an ULK1-dependent manner. *Front Cell Develop Biol*. 2021;9:712124. doi:10.3389/fcell.2021.712124
216. Nam KH, Yi SA, Nam G, et al. Identification of a novel S6K1 inhibitor, rosmarinic acid methyl ester, for treating cisplatin-resistant cervical cancer. *BMC Cancer*. 2019;19(1):773. doi:10.1186/s12885-019-5997-2
217. Zhang L, Fu L, Zhang S, et al. Discovery of a small molecule targeting ULK1-modulated cell death of triple negative breast cancer in vitro and in vivo. *Chem Sci*. 2017;8(4):2687–2701. doi:10.1039/C6SC05368H
218. Li C, Xu H, Chen X, et al. Aqueous extract of clove inhibits tumor growth by inducing autophagy through AMPK/ULK pathway. *Phytoth Res*. 2019;33(7):1794–1804. doi:10.1002/ptr.6367
219. Ye X, Zhou XJ, Zhang H. Exploring the role of autophagy-related gene 5 (ATG5) yields important insights into autophagy in autoimmune/autoinflammatory diseases. *Front Immunol*. 2018;9:2334. doi:10.3389/fimmu.2018.02334

220. Kadowaki M, Karim MR. Cytosolic LC3 ratio as a quantitative index of macroautophagy. *Methods Enzymol*. 2009;452:199–213.
221. Tanida I, Ueno T, Kominami E. LC3 conjugation system in mammalian autophagy. *Int J Biochem Cell Biol*. 2004;36(12):2503–2518. doi:10.1016/j.biocel.2004.05.009
222. Kabeya Y, Mizushima N, Ueno T, et al. LC3, a mammalian homologue of yeast Apg8p, is localized in autophagosome membranes after processing. *EMBO J*. 2000;19(21):5720–5728. doi:10.1093/emboj/19.21.5720
223. Dooley HC, Razi M, Polson HE, Girardin SE, Wilson MI, Tooze SA. WIPI2 links LC3 conjugation with PI3P, autophagosome formation, and pathogen clearance by recruiting Atg12–5-16L1. *Molecular Cell*. 2014;55(2):238–252. doi:10.1016/j.molcel.2014.05.021
224. Mackeh R, Perdiz D, Lorin S, Codogno P, Poüs C. Autophagy and microtubules–new story, old players. *J Cell Sci*. 2013;126(5):1071–1080. doi:10.1242/jcs.115626
225. Klionsky DJ, Eskelinen E-L, Deretic V. *Autophagosomes, Phagosomes, Autolysosomes, Phagolysosomes, Autophagolysosomes… Wait, I'm Confused*. Vol. 10. Taylor & Francis; 2014:549–551.
226. Kudriaeva AA, Sokolov AV, Belogurov AAJ. Stochastics of degradation: the autophagic-lysosomal system of the cell. *Acta naturae*. 2020;12 (1):18–32. doi:10.32607/actanaturae.10936
227. Xia Y, Shen S, Verma IM. NF-κB, an active player in human cancers. *Cancer Immunol Res*. 2014;2(9):823–830. doi:10.1158/2326-6066.CIR-14-0112
228. Hoesel B, Schmid JA. The complexity of NF-κB signaling in inflammation and cancer. *Mol Cancer*. 2013;12(1):86. doi:10.1186/1476-4598-12-86
229. Cartwright T, Perkins NDL, Wilson C. NFKB1: a suppressor of inflammation, ageing and cancer. *FEBS J*. 2016;283(10):1812–1822. doi:10.1111/febs.13627
230. Concetti J, Wilson CL. NFKB1 and Cancer: friend or Foe? *Cells*. 2018;7(9):133. doi:10.3390/cells7090133
231. Zilfou JT, Lowe SW. Tumor suppressive functions of p53. *Cold Spring Harbor Perspect. Biol*. 2009;1(5):a001883–a001883. doi:10.1101/cshperspect.a001883
232. Jin S. Autophagy and tumor suppression. *Autophagy*. 2005;1(3):171–173. doi:10.4161/auto.1.3.2051
233. Lowe JM, Menendez D, Bushel PR, et al. p53 and NF-κB coregulate proinflammatory gene responses in human macrophages. *Cancer Res*. 2014;74(8):2182–2192. doi:10.1158/0008-5472.CAN-13-1070
234. Salminen A, Hyttinen JM, Kauppinen A, Kaarniranta K. Context-dependent regulation of autophagy by IKK-NF- κ B signaling: impact on the aging process. *Int J Cell Biol*. 2012;2012:1–15. doi:10.1155/2012/849541
235. Mi W, Wang C, Luo G, et al. Targeting ERK induced cell death and p53/ROS-dependent protective autophagy in colorectal cancer. *Cell Death Discovery*. 2021;7(1):375. doi:10.1038/s41420-021-00677-9
236. Zhao X, Jiang K, Liang B, Huang X. Anticancer effect of xanthohumol induces growth inhibition and apoptosis of human liver cancer through NF-κB/p53-apoptosis signaling pathway. *Oncol Rep*. 2016;35(2):669–675. doi:10.3892/or.2015.4455
237. White E. Autophagy and p53. *Cold Spring Harb Perspect Med*. 2016;6(4):a026120. doi:10.1101/cshperspect.a026120
238. Rahman MA, Park MN, Rahman M, et al. p53 modulation of autophagy signaling in cancer therapies: perspectives mechanism and therapeutic targets. *Front Cell Develop Biol*. 2022;10:761080. doi:10.3389/fcell.2022.761080
239. Gugnoni M, Sancisi V, Manzotti G, Gandolfi G, Ciarrocchi A. Autophagy and epithelial–mesenchymal transition: an intricate interplay in cancer. *Cell Death Dis*. 2016;7(12):e2520–e2520. doi:10.1038/cddis.2016.415
240. Ribatti D, Tamma R, Annese T. Epithelial-mesenchymal transition in cancer: a historical overview. *Transl Oncol*. 2020;13(6):100773. doi:10.1016/j.tranon.2020.100773
241. Lu W, Kang Y. Epithelial-mesenchymal plasticity in cancer progression and metastasis. *Dev. Cell*. 2019;49(3):361–374. doi:10.1016/j.devcel.2019.04.010
242. Kaszak I, Witkowska-Piłaszewicz O, Niewiadomska Z, Dworecka-Kaszak B, Ngosa Toka F, Jurka P. Role of cadherins in cancer-a review. *Int J Mol Sci*. 2020;21(20):7624. doi:10.3390/ijms21207624
243. Gottardi CJ, Wong E, Gumbiner BM. E-cadherin suppresses cellular transformation by inhibiting β-catenin signaling in an adhesion-independent manner. *J Cell Biol*. 2001;153(5):1049–1060. doi:10.1083/jcb.153.5.1049
244. T-Y N, Schecterson L, Mendonsa AM, Gumbiner BM. The functional activity of E-cadherin controls tumor cell metastasis at multiple steps. *Proc Natl Acad Sci*. 2020;117(11):5931–5937. doi:10.1073/pnas.1918167117
245. Wang Y, Shi J, Chai K, Ying X, Zhou BP. The role of snail in EMT and tumorigenesis. *Curr Cancer Drug Targets*. 2013;13(9):963–972. doi:10.2174/15680096113136660102
246. Usman S, Waseem NH, Nguyen TKN, Mohsin S. Vimentin is at the heart of epithelial mesenchymal transition (EMT) Mediated metastasis. *Cancers*. 2021;13(19):4985. doi:10.3390/cancers13194985
247. Jonckheere S, Adams J, De Groote D, Campbell K, Berx G, Goossens S. Epithelial-mesenchymal transition (EMT) as a therapeutic target. *Cells Tissues Organs*. 2022;211(2):157–182. doi:10.1159/000512218
248. Hui San S, Ching Ngai S. E-cadherin re-expression: its potential in combating TRAIL resistance and reversing epithelial-to-mesenchymal transition. *Gene*. 2024;909:148293. doi:10.1016/j.gene.2024.148293
249. Takeda T, Tsubaki M, Matsuda T, et al. EGFR inhibition reverses epithelial-mesenchymal transition, and decreases tamoxifen resistance via Snail and Twist downregulation in breast cancer cells. *Oncol Rep*. 2022;47(6):1–13. doi:10.3892/or.2022.8320
250. Mazumdar S, Chitkara D, Mittal A. Exploration and insights into the cellular internalization and intracellular fate of amphiphilic polymeric nanocarriers. *Acta Pharmaceutica Sinica B*. 2021;11(4):903–924. doi:10.1016/j.apsb.2021.02.019
251. Qiu C, Xia F, Zhang J, et al. Advanced strategies for overcoming endosomal/lysosomal barrier in nanodrug delivery. *Research*. 2023;6:0148. doi:10.34133/research.0148
252. Aibani N, Rai R, Patel P, Cuddihy G, Wasan EK. Chitosan nanoparticles at the biological interface: implications for drug delivery. *Pharmaceutics*. 2021;13(10):1686. doi:10.3390/pharmaceutics13101686
253. Rathore B, Sunwoo K, Jangili P, et al. Nanomaterial designing strategies related to cell lysosome and their biomedical applications: a review. *Biomaterials*. 2019;211:25–47. doi:10.1016/j.biomaterials.2019.05.002
254. Yang JM, Wu LJ, Lin MT, et al. Construction and evaluation of chitosan-based nanoparticles for oral administration of exenatide in type 2 diabetic rats. *Polymers*. 2022;14(11). doi:10.3390/polym14112181

255. Jin H, Pi J, Yang F, et al. Folate-chitosan nanoparticles loaded with ursolic acid confer anti-breast cancer activities in vitro and in vivo. *Sci Rep*. 2016;6(1):30782. doi:10.1038/srep30782
256. Campoccia D, Ravaioli S, Santi S, et al. Exploring the anticancer effects of standardized extracts of poplar-type propolis: in vitro cytotoxicity toward cancer and normal cell lines. *Biomed. Pharmacother.* 2021;141:111895. doi:10.1016/j.biopha.2021.111895
257. Hadjzadeh M-A-R, Ghanbari H, Keshavarzi Z, Tavakol-Afshari J. The effects of aqueous extract of Alpinia galangal on gastric cancer cells (AGS) and L929 cells in vitro. *Iran J Cancer Prev*. 2014;7(3):142–146.
258. Chang M-C, J-Y W, Liao H-F, Chen Y-J, Kuo C-D. Comparative assessment of therapeutic safety of norcantharidin, N-farnesyloxy-norcantharimide, and N-farnesyl-norcantharimide against Jurkat T cells relative to human normal lymphoblast: a quantitative pilot study. *Medicine*. 2016;95(31):e4467–e4467. doi:10.1097/MD.0000000000004467
259. Gavas S, Quazi S, Karpiński TM. Nanoparticles for cancer therapy: current progress and challenges. *Nanoscale Res Lett*. 2021;16(1):173. doi:10.1186/s11671-021-03628-6
260. Nalezinková M. In vitro hemocompatibility testing of medical devices. *Thromb Res*. 2020;195:146–150. doi:10.1016/j.thromres.2020.07.027
261. Weber M, Steinle H, Golombek S, et al. Blood-contacting biomaterials: in vitro evaluation of the hemocompatibility. *Front Bioeng Biotechnol*. 2018;6:99. doi:10.3389/fbioe.2018.00099
262. Kuchinka J, Willems C, Telyshev DV. Control of blood coagulation by hemocompatible material surfaces-a review. *Bioengineering*. 2021;8(12). doi:10.3390/bioengineering8120215
263. Li X, Wang L, Fan Y, Feng Q, Cui F-Z. Biocompatibility and toxicity of nanoparticles and nanotubes. *J Nanomater*. 2012;2012:6–6.
264. Malehmir S, Esmaili MA, Mahabady MK, et al. A review: hemocompatibility of magnetic nanoparticles and their regenerative medicine, cancer therapy, drug delivery, and bioimaging applications. *Front Chem*. 2023;11:1249134. doi:10.3389/fchem.2023.1249134